NTNU
Innovation and Creativity

Suppression of Radar Echoes produced below the Liquid Surface close to the Base of a Storage Container for LNG

Arne Helge Andersen

Master of Science in Electronics
Submission date: June 2007
Supervisor: Jon Anders Langen Aas, IET
Co-supervisor: Øyvind Jensen, Kongsberg Maritime

Norwegian University of Science and Technology
Department of Electronics and Telecommunications

Problem Description

Radarinstrumenter for nivåmåling av LNG (Liquefied Natural Gas) benytter bølgeleder til å føre radarsignalet ned
mot væska og tilbake til instrumentet. Bølgelederen kan av praktiske årsaker ikke
gå helt ned til bunnen av tanken og når væskenivået blir lavere enn den åpne bølgelederavslutningen,
vil ekkoet fra væskeoverflata kunne forstyrres av ekkoet fra bunnen av tanken. Oppgaven omfatter en teoretisk og praktisk undersøkelse av enkle konstruksjoner for å redusere ekkoet fra bunnen av LNG-tanken.

1. Det skal gjennomføres en teoretisk undersøkelse og behandling av stealth-teknologien. I denne forbindelsen er det naturlig å vinkle undersøkelsen og behandlingen mot aspekter som anses relevante i forhold til den konkrete problemstillingen.

2. Det antas at strålingsegenskapene til åpningen i enden av målerøret får betydning for den endelige løsningen,
og det er derfor ønskelig at de spesifikke utfordringene som ligger i bølgeutbredelsen fra røret blir undersøkt og
vurdert. Undersøkelsen bør tuftes på teoretisk innsikt og analyse, og gjerne med støtte i simuleringer (Agilent HFSS e.l.).

3. Den teoretiske undersøkelsen skal munne ut i et konkret forslag til en konstruksjon som er ansett som lovende med hensyn til å undertrykke bunnekkoet. Konstruksjonen bør ta sikte på at ytelsene endres minst mulig når de ulike konstruksjonsparametrene endrer seg innenfor et " naturlig variasjonsområde" (materialparametre, ulike geometriske størrelser).

4. Det skal bygges en bunnabsorbent som kan testes i laboratoriet. Tilgangen på LNG kan være et problem, og konstruksjonen bør derfor tilpasses en annen og lettere tilgjengelig væske.

Den teoretiske og praktiske gjennomføringen av oppgaven vil bli delt mellom instituttet og Kongsberg Maritime AS slik det faller formålstjenlig.

Assignment given: 15. January 2007
Supervisor: Jon Anders Langen Aas, IET

Suppression of radar echoes produced below the liquid surface close to the base of a storage container for LNG.

Arne Helge Andersen

June 19, 2007

Preface

This assignment was written during the spring 2007 at Department of Electronics and Telecommunications at NTNU as the final thesis of the Master of Science degree in Electronics.
The assignment is given by Kongsberg Maritime and is a continuance of a prestudy done by the undersigned at NTNU autumn 2006. Most of the work is done at NTNU Trondheim besides the tests done on the end product. These were done at Kongsberg Maritime R&D department in Trondheim.

I would like to thank Øyvind Jensen who is the proposer of this assignment and my supervisor at Kongsberg Maritime. He has been at good help providing me with earlier research notes and answering questions which rose during the semester. He also arranged and helped out during the test and analysis of the bottom absorber. I also want to give a special thanks to Jon Anders Aas for being my contact person at NTNU. He has contributed by answering and explain my theoretical questions during this semester.

Last but not least I want to say thanks to Nilz Leksir for invaluable support, motivation and catchy mood during my years in Trondheim.

Trondheim, June 19, 2007

Arne Helge Andersen

Contents

1 Introduction **1**

1.1 The Level Gauge System 1

1.2 Problems 3

2 Theory **5**

2.1 EM Fundamentals 5

2.1.1 Wave Propagation 5

2.1.2 Loss mechachanism 6

2.1.3 Reflection 7

2.2 Radar 9

2.2.1 Radar Cross Section 9

2.3 Radar Cross Section Reduction 10

2.3.1 Shaping 10

2.3.2 Radar absorbing material 11

2.4 System description FMCW Radar 12

2.4.1 Basic principles of FMCW Radar 13

3 Bottom Absorber **15**

3.1 Design 16

3.2 Thickness 17

3.2.1 Ideal Thickness 17

3.2.2 Practical Thickness 18

3.3 Combination 19

3.3.1 Combination ratio for LNG 19

3.3.2 Combination ratio for paraffin 20

4 Simulation **23**

4.1 Model 24

4.2 EMDS Simulation 26

4.2.1 LNG . . . 26
4.2.2 Paraffin . . . 30
4.3 Error analysis . . . 32

5 Testing **35**
5.1 Creation of Bottom Absorber . . . 35
5.2 Measurement set-up . . . 36
5.3 Measurement against air . . . 38
5.3.1 The echo signal . . . 38
5.3.2 Bottom absorber impedance calculations . . . 41
5.4 Measurements with paraffin . . . 45

6 Discussion **49**
6.1 Thickness . . . 49
6.2 Permittivity of paraffin . . . 50
6.3 Bottom absorber calculations . . . 50
6.4 Input impedance of the bottom absorber . . . 51

7 Conclusion **55**
7.1 Future Work . . . 55

A Appendix **59**
A.1 Derivation of Input Impedance [6,p299-300]. . . . 59
A.2 Simulation . . . 60
A.2.1 Currents in bottom absorber . . . 60
A.2.2 E-field near bottom in simulation model . . . 61
A.2.3 S11 for paraffin with ideal ratio . . . 61
A.3 Matlab code . . . 62
A.3.1 Input Impedance of RAM . . . 62
A.3.2 Combination calculations . . . 63
A.3.3 Measurements with air . . . 64
A.3.4 Measurements with paraffin . . . 67
A.3.5 Validation for testing against air . . . 69
A.4 Data Sheet RAM . . . 70

List of Figures

1.1 Level gauge setup 2
1.2 Bottom bucket 3
1.3 Anti-phase step 3

2.1 Block diagram 12
2.2 Measured data with a certain number of periodes 13

3.1 Structure of bottom absorber 16
3.2 Input Impedance of RAM at 10GHz 18
3.3 Input Impedance of RAM at 10GHz with fixed thickness 19
3.4 Combination ratio in LNG for t=2.00mm and t=6.00mm 21
3.5 Combination ratio in paraffin for t=2.00mm and t=6.00mm 21

4.1 E field concentration around the step 23
4.2 Simulation Model 24
4.3 E field in model 26
4.4 Bottom design Type 1 for LNG 27
4.5 S11 parameters for Type 1 bottom absorber designed for LNG 27
4.6 Path loss in model with LNG 28
4.7 Bottom design Type 2 for LNG 28
4.8 S11 parameters for Type 2 bottom absorber designed for LNG 29
4.9 Bottom design Type 1 for paraffin 30
4.10 S11 parameters for Type 1 bottom absorber designed for paraffin . . 30
4.11 S11 parameters for Type 2 bottom absorber designed for paraffin . . 31
4.12 Path loss in model with paraffin 31
4.13 Polarization test Type1 32
4.14 Offset test Type1 33
4.15 Polarization test Type2 33
4.16 Offset test Type2 34

5.1 The end result. Type2 on top, Type1 at the bottom. 36
5.2 Measurement set-up 37
5.3 Bucket with bottom absorber. 37
5.4 Normal reflection from an metal plate in the time domain. 38
5.5 Prosessed echo signal 39
5.6 Theoretical values for the set-up 40
5.7 42
5.8 Input impedance for the bottom absorber 43
5.9 Echo strength at different levels. 46
5.10 Difference plot 46
5.11 Echo from subnerged bottom absorber 47

6.1 Resonant circuits 49
6.2 Validation of air measurements 51
6.3 Input impedance vs SWR 53

A.1 E-field near bottom 61
A.2 S11 for paraffin with ideal ratio 61

List of Tables

3.1 Thickness vs Input Impedance 17
3.2 Input Impedance for fixed thickness 18
3.3 Thickness vs Reflection in LNG 20
3.4 Thickness vs Reflection in Paraffin 20

5.1 Measurements with paraffin 45

List of Abbreviations

ANA Automatic Network Analyzer

CW Continous Wave

EM Electromagnethic

EMDS Electromagnetic Design System

FMCW Frequency Modulated Continuous Wave

LNG Liquefied Natural Gas

LO Local Oscillator

RADAR Radio Detection and Ranging

RAM Radar Absorbent Material

RCS Radar Cross Section

RCSR Radar Cross Section Reduction

RF Radio Frequency

Summary

In this document designing a bottom absorber used in a level gauge system is discussed. The bottom absorber is placed in the bottom of a tank and its task to attenuate the signal reflected by the bottom in such a way that the wanted echo can be sensed. The bottom absorber used today can give measurement errors due to wrong installation.

The design is done on the basis shown in this paper and from experience accomplished in my pre-study. The idea is to combine Radar Absorbing Material with different thicknesses at a certain ratio. With this approach the input impedance of the bottom absorber can be designed to agree with impedance of the media above. This leads to low reflection at the interface and energy consumption in the absorber. The thickness of the RAM and its combination ratio was theoretically calculated and then simulated with the help of Agilent EMDS.

The results from the real life testing was quite pleasant. The design makes it possible to match the bottom absorber to the wanted reference medium. The bottom absorber will then have good qualities regarding attenuation of the incident signal.

Chapter 1

Introduction

The idea of reducing radar backscatter is very old and it has been investigated more or less since the birth of the radar. To get control over and be able to reduce radar backscatter can have many purposes. The most obvious is the evolution of stealth technology used in military fighter aircraft, boats, vehicles and other military equipment. When used in such device the main goal is to hide from the enemy radar.

This technology with reducing the radar backscatter can also be utilized in commercial equipment. This paper will take a look at a level gauge system which is used to measure the level of Liquefied Natural Gas (LNG) in a tank.

1.1 The Level Gauge System

To get a better understanding of the problem, this section will give a short description of the level gauge system as it is today.

The gauge system which is going to be investigated in this assignment is used for measuring the level of LNG in a tank. Inside a LNG tank the environment is quite harsh. To transport LNG, the gas is turned into fluid which is done at a temperature of approximately -162°C. The LNG is highly explosive, so the amount of energy allowed inside the tanks is very low.

The liquid level in the tank is measured with the help of a Frequency Modulated Continuous Wave Radar (FMCW) Radar placed on top of the tank. The radar signal propagates in a wave-guide until approximately 150mm above the bottom of the tank. From here it propagates towards the liquid, reflects from the surface, and then back to the radar detector. The actual distance from the radar to the surface, hence also the level of liquid in the tank, is done by measure the actual phase difference between the transmitted and received signal. More about the actual measuring technique in subsequent chapters.

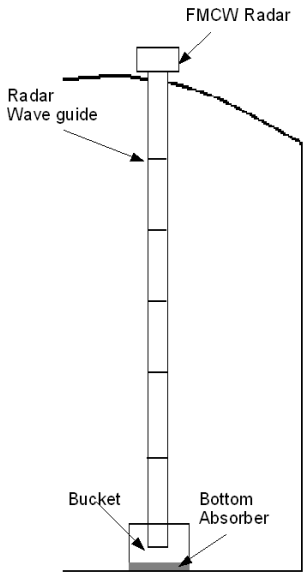

Figure 1.1: Level gauge setup

Under the radar wave guide a bucket is placed to reduce waves on the liquid surface which can deflect the radar signal away from the detector. As the LNG is very transparent a bottom absorber is needed to attenuate the unwanted backscatter from the bottom of the tank. It is placed as shown in figure 1.2

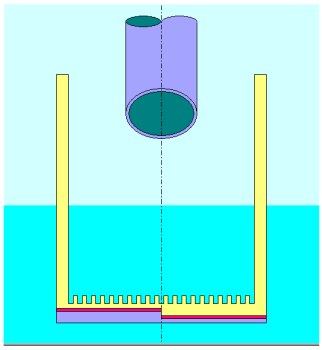

Figure 1.2: Bottom bucket

The bottom absorber used today is mainly based on a anti-phase step as shown in figure 1.3. The step has an electrical length equal to the quarter of a wavelength in the given medium. This leads to a phase shift of 180 ° and hence also destructive interference. To extinguish the backscattered energy from the bottom part, similar amount of energy is needed from both sides of the step. This implies strict symmetry around the step which again implies a hard time when coming to install the bottom absorber.

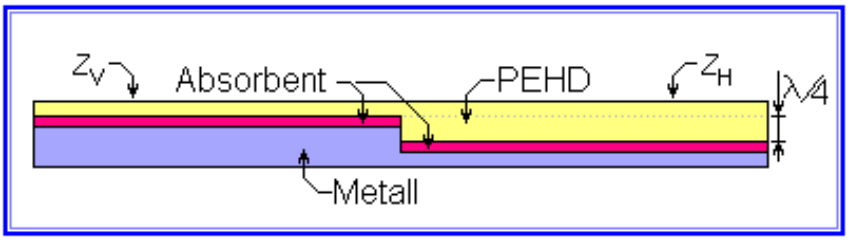

Figure 1.3: Anti-phase step

1.2 Problems

With the harsh environment caused by the LNG, to design a bottom absorber implies a lot of challenges.

One known technology to reduce radar backscatter is the use of radar absorbing material. This is often developed to interact with the impedance of air or vacuum. In this paper we are working with medias which have different impedance compared to air. If the RAM is not tuned to match its reference media, it will cause a reflection from the interface of the two materials. The RAM should also be able to manage the temperatures exposed to it.

As mentioned a anti phase technology is used today. This require accuracy

when coming to installing the absorber so that the step is straight under the middle of the symmetry line of the wave guide. To reduce the installation difficulties a non symmetric substrate is wanted.

To summarize, the purpose of this paper is to investigate and design a substrate which placed in the bottom of a tank will attenuate the radar signal sufficient so that the unwanted backscatter dont interfere with the surface echo. It is also wanted that the designed is without any needs of symmetry and that it is as thin as possible.

Chapter 2

Theory

To get a deeper understanding of the problem, the theory regarding the phenomenas which is present in the system is a useful place to start. This chapter will deal with some of the basic theory but it is still expected that the reader have a basic knowledge of wave propagation and electromagnethics (EM).

2.1 EM Fundamentals

2.1.1 Wave Propagation

In our electromagnetic world there are some universal constants, for instance velocity of electromagnetic waves in free space c, permittivity of free space ϵ_0 and permeability of free space μ_0 [1].
Their relationship are:

$$c = \frac{1}{\sqrt{\epsilon_0 \mu_0}} \quad [m/s] \tag{2.1}$$

The permeability of free space is

$$\mu_0 = 4\pi \cdot 10^{-7} \quad [H/m] \tag{2.2}$$

hence the permittivity of free space can be derived from (1)

$$\epsilon_0 \cong 8.854 \cdot 10^{-12} \quad [F/m] \tag{2.3}$$

Permittivity ϵ, characterize a materials ability to store electrical energy and permeability μ, characterizes a materials ability to store magnetic energy [2].

As the the wave propagates from one medium to another the wave will reduce or increase its velocity, depending on the characteristic of the media. Its speed in a given media is given by [3]:

$$v = \frac{1}{\sqrt{\epsilon\mu}} \tag{2.4}$$

When propegating in a circular waveguide the velocity is reduced and can be representated as [4]:

$$v = \frac{c}{\epsilon_r} \cdot \sqrt{\epsilon_r - \left(\frac{S}{D \cdot f}\right)^2} \tag{2.5}$$

where in this case S = $1.757 \cdot 10^8 m/s$
The wave impedance is then [1]:

$$Z = \frac{\eta}{\sqrt{\epsilon_r - \left(\frac{S}{D \cdot f}\right)^2}} \tag{2.6}$$

where η is the intrinsic impedance of the guide medium.

The wavelength of an EM wave is dependent of the frequency and in which media it propagates (at which speed).
This relation is given by:

$$v = \frac{\lambda}{T} = \lambda f \Longrightarrow \lambda = \frac{v}{f} = \frac{1}{f \cdot \sqrt{\epsilon\mu}} \tag{2.7}$$

The ratio of the speed of an EM wave in vacuum to its speed in a medium is called the refractive index of the medium and is given as:

$$n = \frac{c}{v} = \frac{\sqrt{\epsilon\mu}}{\sqrt{\epsilon_0\mu_0}} = \sqrt{\epsilon_r\mu_r} \tag{2.8}$$

2.1.2 Loss mechachanism

In addition to conductive losses σ, materials have dielectric and magnetic losses [5]. When a normal material is present in a time-varying field its response will depend on the frequency of the field. Charged particles in the material will try to vary with the same frequency as the applied field. With increased frequency the fluctuations of the particles in the material and the applied field will be out of phase. The

inertia of the charged particles in the material tends to prevent the particle displacement from keeping in phase with the time-varying field. This leads to a frictional damping mechanism that causes power loss due to the work that must be done to overcome the damping forces [1].

The out of phase phenomena can be characterized by a complex electric susceptibility. This, in combination with ohmic losses, leads to a complex permittivity.

$$\epsilon_r = \epsilon_r^{'} - j\epsilon_r^{''} \tag{2.9}$$

In an ideal dielectric the voltage and current is 90° out of phase and there is no current in-phase with the voltage. If a material with a certain dielectric constant ϵ_r is placed in an electrical field another situation will occur.
The current will now have components in-phase with the voltage.
$\epsilon_r^{'}$ has a influence on the component of the current that is out of phase with the voltage and $\epsilon_r^{''}$ has an influence on the in-phase component of the current.
$\epsilon_r^{''}$ is usually referred to as the loss factor [6]

Similar loss arguments can be applied regarding magnetization. It is expected that the permeability will be complex at high frequencies and is expressed as [1]:

$$\mu_r = \mu_r^{'} - j\mu_r^{''} \tag{2.10}$$

Relative permittivity ϵ_r, and relative permeability μ_r are normalized by the free-space values $\epsilon_0$andμ_0, and have a complex notation as explained above.

2.1.3 Reflection

In an attempt to minimize the reflection from given surface it could be useful to take a look at some of the physical equations that represent the reflection process.

One of the main equation describes the reflection coefficient at a given interface [7]:

$$\Gamma = \frac{Z - Z_0}{Z + Z_0} \tag{2.11}$$

An important special case results when the reflection coefficient is 0. It is then said that we have an impedance match [8].

The intristic impedance of a material is given by:

$$Z = \sqrt{\frac{\mu_r \cdot \mu_0}{\epsilon_r \cdot \epsilon_0}} \tag{2.12}$$

If there is a perfect impedance match at a given interface there will be no reflection from the boundary of the incident media and all the energy of the wave will be transmitted into the new media. If the receiving media is of the lossy kind, the wave can be attenuated as it propagates through the media. A uniform plane wave propagating in the z direction can be representated by:

$$\mathbf{E} = \mathbf{a}_x \mathbf{E}_x \ = \ \mathbf{a}_x E_0 e^{-\gamma z} \tag{2.13}$$

For a plane wave in lossy media, the propagation constant gamma, γ, can be given as [1]:

$$\gamma = \alpha + j\beta = j\omega\sqrt{\mu\epsilon'}\left(1 - \frac{\epsilon''}{j\omega\epsilon'}\right)^{1/2} \tag{2.14}$$

Then equation 2.13 can then be expressed as:

$$E_x = E_0 e^{-\alpha z} e^{-j\beta z} \tag{2.15}$$

It shows from the latter equation that the real part will decrease as z increases, thus α is called an attenuation factor. The imaginary part,β, is called a phase constant and expresses the amount of phase shift that occurs as the wave propagates. Both α and β is given per meter.

To get a large amount of attenuation in a small thickness, α must be large, which implies that the real and imaginary part of the permittivity and permeability must be large. It is noted that large values of permittivity and permeability could result in a large reflection coefficient.

If a plane EM wave is incident normal to a plane dielectric boundary and a impedance mismatch is present, the wave is partly reflected and partly transmitted into the new medium [1]. The reflection coefficient and transmission coeffecient can then be representated by:

$$\Gamma = \frac{E_{r0}}{E_{i0}} \tag{2.16}$$

and

$$\tau = \frac{E_{t0}}{E_{i0}} \tag{2.17}$$

where E is respectively the magnitude of the incident, transmitted and reflected wave at the boundary.

2.2 Radar

Radar is a method of using electromagnetic waves to sense the position, velocity and characteristics of a target from a remote position. This is done by by illuminate a volume of space with electromagnetic energy, then sense the energy reflected by the target (echo) [9]. The received power is given by:

$$P_r = \frac{P_t G^2 \lambda^2}{(4\pi)^3 R^4} \cdot \sigma \tag{2.18}$$

where

P_t: the transmitted power

λ: the wavelength of the transmitted signal

G: the antenna gain

σ: the radar cross section

R: the range to the target

The mode and type of radar used is determined by the specific measurement that we want to make and the environment in which it is going to operate. Radars can be classified by the waveform that they transmit and are of two general types; continuous wave (CW) and pulsed wave [10] .

CW radars transmit and receive unmodulated sinusodial waves. The transmitter and receiver operate simultaneously, and the receiver must amplify weak target echoes in the presence of a strong transmitted signal. Except for very low power systems (here), spillover controll dictates the use of separate transmit and receive antennas. CW radar primarily measure the target echo Doppler shift (and therefore radial velocity) and angular position. Range cannot be measured directly without some form of time-variant modulation [1].

2.2.1 Radar Cross Section

Radar cross section (RCS) is defined as:

> the area intercepting that amount of power which, when scattered isotropically, produces at the receiver a density which is equal to that scattered by the actual target [11, pg.96].

Mathematically it can be described:

$$\sigma = \lim_{R \to \infty} 4\pi R^2 \frac{|E_r|^2}{|E_i|^2} \tag{2.19}$$

It is, by definition, independent of the transmitted power, receiver sensitivity and the distance between transmitter and receiver. Another word used for RCS is echo area.

If a target is subdivided into N discret scatters the sum of all scatters can be represented as [2].

$$\sigma = \left| \sum_n \sqrt{\sigma_n} e^{j\phi_n} \right|^2 \tag{2.20}$$

where σ_n is the backascatter of the nth scatter and ϕ_n is realtive phase diference.

As could be seen from the radar equation, the received power is directly proportional to the radar cross section σ. This direct influence on the received power and its independence from other elements, are the reasons why radar cross section reduction (RCSR) is very interesting when coming to design a surface with low backscatter.

2.3 Radar Cross Section Reduction

There are only four basic techniques for reducing radar backscatter [2]

- Shaping
- Radar Absorbing Materials (RAM)
- Passive cancellation
- Active cancellation

All of the above mentioned methods of radar backscatter suppression have their advantages and disadvantages. Most common and practical are shaping and the use of radar absorbing materials.

2.3.1 Shaping

Shaping lets us, at a certain amount, control the reflected energy from the object. The main goal is to prevent the energy from propagate back toward the radar detector. This can be done by orientating the target surface in such way that the energy is scattered away from the radar detector.

2.3.2 Radar absorbing material

RAM is based on the simple fact that some materials exposed to an electromagnetic field absorb energy. It is possible to look at the the energy consumption, the dissapation of energy or power, the same way as in a regular resistor. The loss is a transformation from electrical energy into heat [2].
The energy that dissapate is said to be absorbed by the media. For the media to be an effective absorber the electric loss tangent shuld be as large as possible [12].
It can be described as:

$$tan\delta_e = \frac{\sigma_c + \omega\epsilon^{''}}{\omega\epsilon^{'}} \tag{2.21}$$

Similar describtion can be given for the magnetic loss tangent.
Different types of RAM are been characterized by their permittivity and permeability. The real part represent energy storage and the actual loss is, as mentioned earlier, determined by their imaginary components, respectively $\epsilon^{''}$ and $\mu^{''}$.

In general it can be said that:

- Magnetic properties increase the bandwidth of absorbers.
- High dielectric constant reduces bandwidth.

To find the input impedance of the absorbing material when backed by a conducting surface, the formulas from transmission line analysis can be used. It can be shown that the input impedance is given as[1]:

$$Z_i = Ztanh(jwT\sqrt{\epsilon\mu}) \tag{2.22}$$

where
Z is the intrinsic impedance
w is the angular frequency
T is the thickness of the absorbing material

[1] for derivation see appendix

2.4 System description FMCW Radar

Introducing time-variant modulation on the CW wave adds the capability to directly find target range. This system uses a frequency modulation with a linear sweep from 9 to 11 GHz.

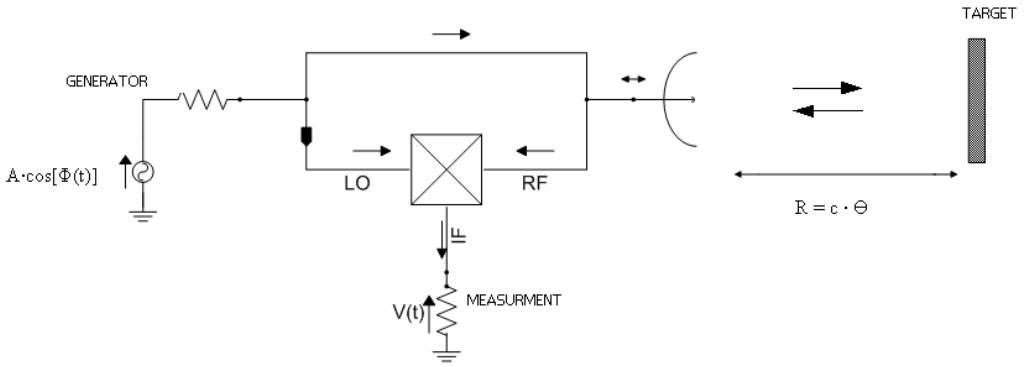

Figure 2.1: Block diagram

Due to different pathway for the echo signal RF and the reference signal LO, a phase difference will occure. This phase difference is proportional with the radar frequency. Changes in the phase difference is measured in the detector (in principle when the echo signal and the reference signal is at the same frequency).

Signal	*Phase*
$LO \approx A \cdot \cos[\Phi(t)]$	$\Phi(t) = \Phi_0 + \omega \cdot t$
$RF \approx A \cdot \cos[\Phi(t - 2 \cdot \theta)]$	$\Phi(t - 2 \cdot \theta) = \Phi_0 + \omega \cdot t - 2 \cdot \omega \cdot \theta$
$IF \approx A \cdot \cos[\Phi(t) - \Phi(t - 2 \cdot \theta)]$	$\Phi(t) - \Phi(t - 2 \cdot \theta) = 2 \cdot \omega \cdot \theta$

$$V(t) \approx IF \approx A \cdot \cos[2 \cdot \omega \cdot \theta] \tag{2.23}$$

The output signal V(t) of the detector will be sinousodial as shown in figure 2.2. The number of periodes in the output signal is a measure of accumulated phase and hence also a measure of the pathway difference betweeen the echo and reference signal [13].

The measured signal V(t) can be representated on its comlex form and can be regarded as a sum of the negative and positive vector rotating in respectively positive and negative direction in the complex plane:

$$\cos(2\omega\theta) = \frac{1}{2} \cdot e^{j \cdot 2\omega\theta} + \frac{1}{2} \cdot e^{-j \cdot 2\omega\theta} \tag{2.24}$$

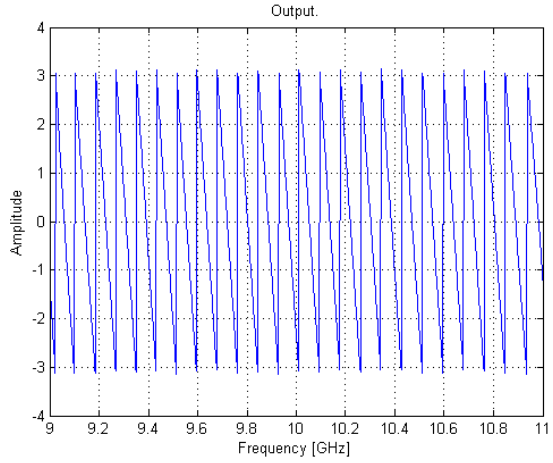

Figure 2.2: Measured data with a certain number of periodes

To be able to find the range a modulation is used, here a linear sweep with N steps.

$$\omega = \omega_0 + \Delta\omega \frac{n}{N} \qquad 1 \leq n \leq N \tag{2.25}$$

which leads to [1]

$$2\omega\theta = 2\omega_0\theta + 2\pi \cdot P \cdot \frac{n}{N} \tag{2.26}$$

where P represents the total number of rotations accumulatet during one sweep. The rotation time of one cycle in the complex plane can be expressed as $2\pi/\Delta\omega$ = $2{\cdot}\Delta\theta$. All this leds to the possibility to determine the echo flight time

$$\theta = \Delta\theta \cdot P = \frac{\pi}{\Delta\omega} \cdot P \tag{2.27}$$

To determine the one way flight time, P has to be measured and equation 2.27 has to be divided by the double bandwith $2\Delta f$ = $\Delta\omega/\ \pi$. The total number of cycles, here representated by P, can be determined by using fourier analysis [14].

2.4.1 Basic principles of FMCW Radar

FMCW Radar technology and fourier trasnform fits like a glove. The time domain and the frequency domain represents the same amount of information. A short time puls Δt contains a wide range of frequencies $\Delta\omega$, and vice verca. The two domains are Fourier transformation pair which gives us

$$\Delta t \cdot \Delta\omega \approx 2\pi \tag{2.28}$$

[1] $2\omega\theta = 2\omega_0\theta + 2\Delta\omega \cdot \Delta\theta \cdot \frac{\theta}{\Delta\theta} \cdot \frac{n}{N}$

Hence if we want a high resolution, which corresponds to a small Δt , a large bandwith must be used. The ideal range resolution can be expressed as [15]:

$$R = \frac{c \cdot \Delta t}{2} = \frac{c}{2 \cdot \Delta \omega} \tag{2.29}$$

Chapter 3

Bottom Absorber

Due to difficulties in installing earlier versions of the bottom absorber, there is a wish for a non symmetric - easy install bottom absorber.
To reduce the backscatter we can, as mentioned in former chapters, use different kinds of techniques. Different shapes and structures can scatter the incident electromagnetic wave, or with help of radar absorbing material we can attenuate the reflected energy.
As always different techniques have different qualities, both positive and negative. The design process is more about electing the qualities that is important in your special case.

As explained earlier a bucket is used to calm down the surface underneath the radar waveguide to give a better control of the backscatter from the surface of the fluid. If a solution with just shaping or scattering is used, it can be difficult to reflect the energy away from the unwanted regions due to the sidewalls of the bucket.

One more concern is that the LNG fluid is very transparent. Only a small percentage of the energy will be reflected from the surface of the fluid, roughly 2 % [1], hence a major part of the energy will be transmitted through the liquid and towards the bottom part of the tank. If no absorbing material is present here, the backscatter is purely due to reflection from a metal surface. This can give rise to high energy backscatter that might interfere and totally conquer the wanted signal from the top of the liquid.

[1] The reflection between air - LNG: $\Gamma = \frac{377-292}{377+292} = 0.127$. This is voltage reflection, the energy is found by taking the square of the absolute value. $|\Gamma|^2 = 0.016$ which is a bit under 2%.

3.1 Design

A way of solving the problem with unwanted backscatter is with use of radar absorbing material. One positive side effect is the fact that a solution with RAM can give a thinner bottom absorber than used today. If the radar resolution and the attenuation from the absorber is good enough, the liquid can then be measured closer towards the bottom.
As known from the electromagnetic theory a leap in impedance will give us a certain reflection from the interface between two materials with different characteristics [7].

> The electromagnetic aspects of RAM design focus principally on the synthesis of an arrangement of dielectric or magnetic materials that provide a specified impedance profile to an incident wave [2, pg. 297]

In this paper the idea is to design and analyze a combination of radar absorbing material with different thickness so that the sum of the reflections from the subsystems will give us less unwanted backscatter. This can be seen as a parallel to equation 2.20 on page 10.

Such a combination of layers can be created with a design as shown in figure 3.1. This design will have an advantageous smooth surface with a certain structure underneath the radar absorbing material.

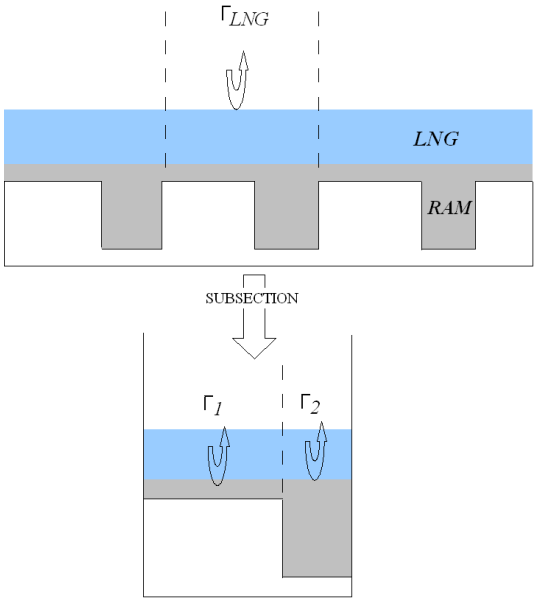

Figure 3.1: Structure of bottom absorber

3.2 Thickness

The idea used here is as mentioned combination of absorbing material with different thickness. Here the material is backed with metal so formula 2.22 on page 11 can be used to find the input impedance. As could be seen from equation 2.22 the input impedance is dependent, amongst other, of the frequency and the characteristic of the RAM. The center frequency of the radar used in this system is 10 GHz thus the thickness is calculated at this frequency.
The RAM provided by Kongsberg Maritime to use in this assignment is of the type SFU-10.0 from Emmerson & Cummings[2].
After research from Kongsberg Maritime its permittivity and permeability is found to be [16]:

$$\epsilon_r = 10.5 \; - \; j\,0.3 \tag{3.1}$$

$$\mu_r = 1.2 \; - \; j0.5 \tag{3.2}$$

3.2.1 Ideal Thickness

Figure 3.2 is a graphical representation of the input impedance of the absorbing material and shows us the real and imaginary parts of the input impedance (Z_{real} and Z_{imag}) for different thicknesses. The liquid above the bottom absorber will have a real input impedance, hence the thickness were Z_{imag} is as close to zero as possible are chosen.

Table 3.1 summarize the values of Z_{real} and T for $Z_{imag} \approx 0$.
The electrical wavelength in the RAM at 10GHz is 8.1mm. As could be seen from

No.	*Thickness (mm)*	*Real component (ohm)*
1.	1.991	415
2.	4.399	84.6
3.	5.805	168.8

Table 3.1: Thickness vs Input Impedance

the values in table 3.1 these are close to $\lambda/4$, $\lambda/2$ and $2 \cdot \lambda/3$.

[2]see appendix for data sheet

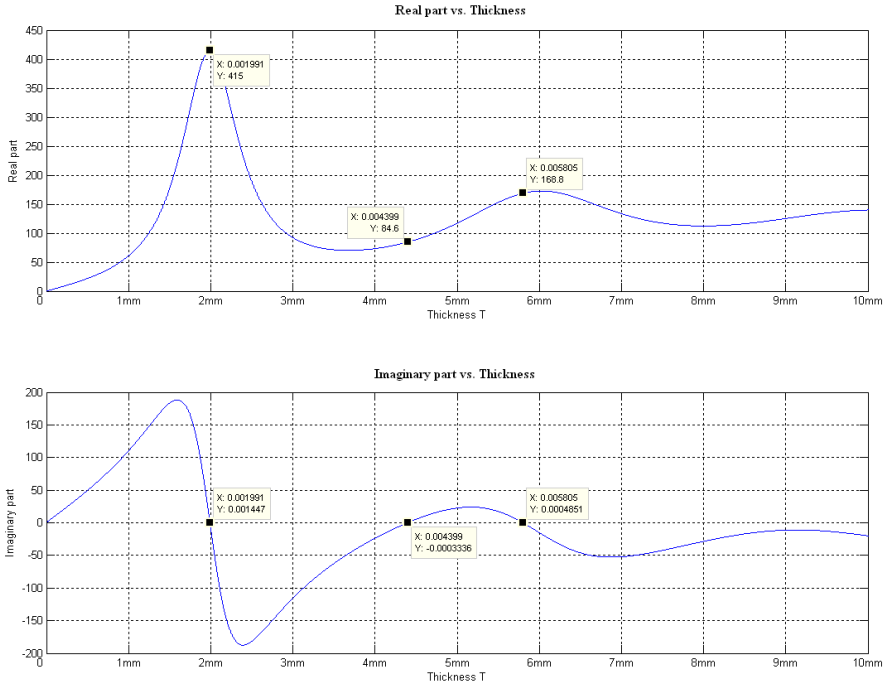

Figure 3.2: Input Impedance of RAM at 10GHz

3.2.2 Practical Thickness

Due to limits from the RAM dealer and other practical issues the thickness of the RAM is set to be 2mm, 4mm and 6mm. This leads to slightly different values when comparing with the ideal values.
With fixed thickness the values in 3.3 are found:

The exact input impedance are calculated using Matlab and summarized in table 3.2. It could be seen that the imaginary part of the input impedance is small compared to the real component.

No.	*Thickness (mm)*	*Input Impedance*
1.	2.00	414.9 - 8.36i
2.	4.00	73.33 - 24.00i
3.	6.00	172.7 - 14.79i

Table 3.2: Input Impedance for fixed thickness

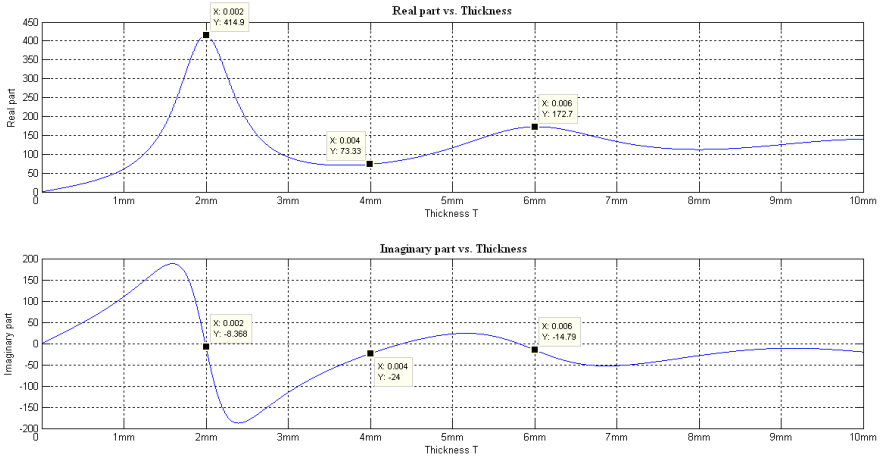

Figure 3.3: Input Impedance of RAM at 10GHz with fixed thickness

3.3 Combination

To reduce the backscatter and design a bottom absorber with the desired characteristics the thicknesses have to be combined at a certain ratio. Some possible combinations can be:

$$Z_1 \cdot k_1 + (1 - k_1) \cdot Z_2 = surface\ impedance \tag{3.3}$$

$$\Gamma_1 \cdot k_2 + (1 - k_2) \cdot \Gamma_2 = summarized\ reflection \tag{3.4}$$

The reflection coefficients are dependent of the media above the absorber. Since at this stage of the project doing real life testing with the use of LNG is impossible, a different fluid is to be used for testing. Here paraffin is used. LNG and paraffin have slightly different characteristics so the combination has to be calculated for both fluids.
Since it is only the practical thicknesses which are going to be further investigated the results with ideal thicknesses are omitted.

3.3.1 Combination ratio for LNG

To find the ratio of combination when designing for LNG the values regarding thickness found in table 3.2 are used. Based om previous experiences the preferred combination is found by using a linear combination of the reflection coefficients shown in equation 3.4. This in combination with thicknesses of 2 and 6mm leads to a bottom absorber wich is more broadband than for other combinations [17].

Each Γ which arises between LNG and the specified RAM at given thicknesses are summarized in table 3.3

Γ_i.	*Thickness (mm)*	Γ
1.	2.00	0.1739 - 0.0098i
3.	6.00	-0.2554 - 0.0400i

Table 3.3: Thickness vs Reflection in LNG

The value of the summarized reflection in equation3.4 should be as close to zero as possible. When using the fixed thicknesses, zero value of the summarized reflection can not be obtained, but a minimum value can be found. This is though possible if only the real part of the reflections are taken under consideration. Since the imaginary parts are small, the approximation with use of only the real parts can be legitimated. By using the real parts of the values in table 3.3 and equation 3.4 the ratio of how to combine the thick and the thin RAM is found.

$$\begin{aligned} \Gamma_1 \cdot k_{2LNG} + (1 - k_{2LNG}) \cdot \Gamma_3 &= 0 \\ 0.4294 \cdot k_{2LNG} &= 0.2554 \\ k_{2LNG} &= 0.5949 \end{aligned} \tag{3.5}$$

This is presented graphical in figure 3.4.

3.3.2 Combination ratio for paraffin

Paraffin has a slightly different impedance from LNG. The ϵ of paraffin is approximately 2.25, which correspond to an input impedance of $Z_{par} = 251\Omega$. To find the ratio of combination, the same procedure as for LNG is followed.

Γ_i.	*Thickness (mm)*	Γ
1.	2.00	0.2462 - 0.0095i
3.	6.00	-0.1833 - 0.0413i

Table 3.4: Thickness vs Reflection in Paraffin

By using the real parts of the values in table 3.4 and equation 3.4 the ratio of how to combine the thick and the thin RAM is found.

$$\begin{aligned} \Gamma_1 \cdot k_{2par} + (1 - k_{2par}) \cdot \Gamma_3 &= 0 \\ 0.4296 \cdot k_{2par} &= 0.1833 \\ k_{2par} &= 0.4268 \end{aligned} \tag{3.6}$$

This is presented graphical in figure 3.5.

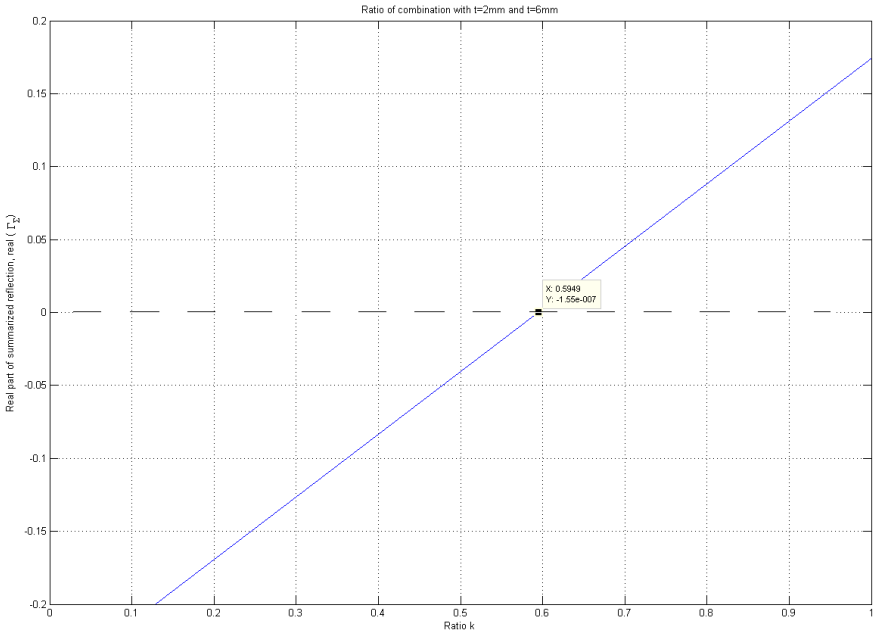

Figure 3.4: Combination ratio in LNG for t=2.00mm and t=6.00mm

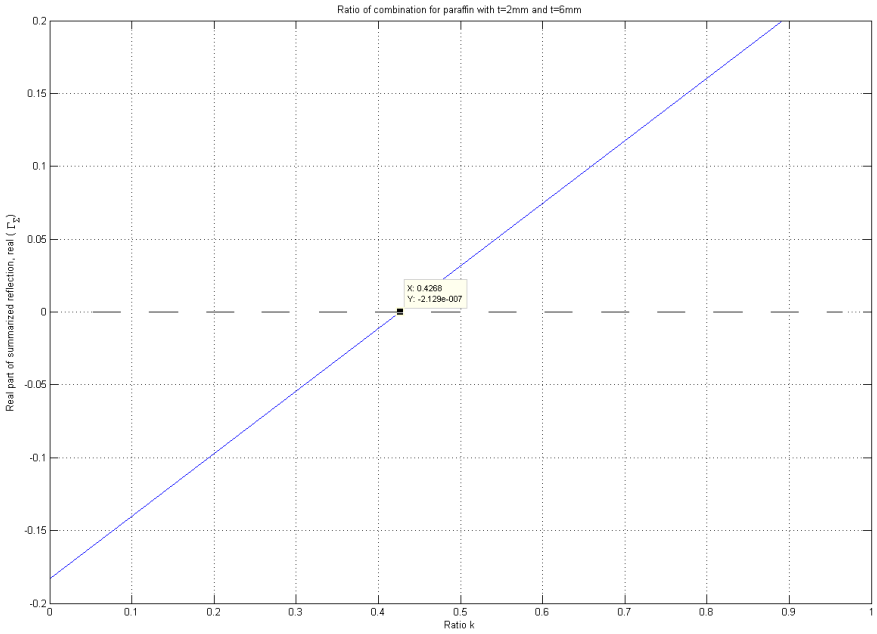

Figure 3.5: Combination ratio in paraffin for t=2.00mm and t=6.00mm

Chapter 4

Simulation

The next step of creating a new easy install bottom absorber is to join the small subsections into a larger model. The sum can be seen as a parallel to equation 2.20 on page 10. Up to now the calculations has been done by considering only one of the subsection. This combination will probably effect the total result. The bottom substrate is constructed out of metal which will lead to currents flowing in the substrate. This will again lead to radiant fields from the bottom absorber which will have an influence on the total backscatter. This is a highly complex interaction, and further theoretical studies of these phenomenas will not be taken into consideration in this assignment. Figure 4 shows the e-field congestion at the step[1]. By doing simulations it is possible to investigate and include these phenomenas in the final design. All the simulations are done with the help of Agilent EMDS.

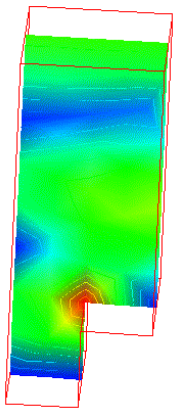

Figure 4.1: E field concentration around the step

[1]More figures regarding the currents in the metal is found in the appendix.

4.1 Model

The creation of a good and rigorous simulation model was a challenge. Before a model with the possibility to extract the wanted information without influence from unwanted construction phenomenas, a more thorough research had to be done.

The way Agilent EMDS works is by dividing a volume into a certain number of smaller tetrahedral volumes in a certain mesh. The field components in each tetrahedron are calculated. If better resolution is wanted, the tetrahedral volumes are decreased, hence there will be a larger amount of them. High resolution thus leads to a large number of calculations which again leads to a need of high computer power and memory. With limited computer power a simple model containing only the most important components was created. It should also be kept in mind that the task of this assignment is to design a bottom absorber and investigate its backscatter.

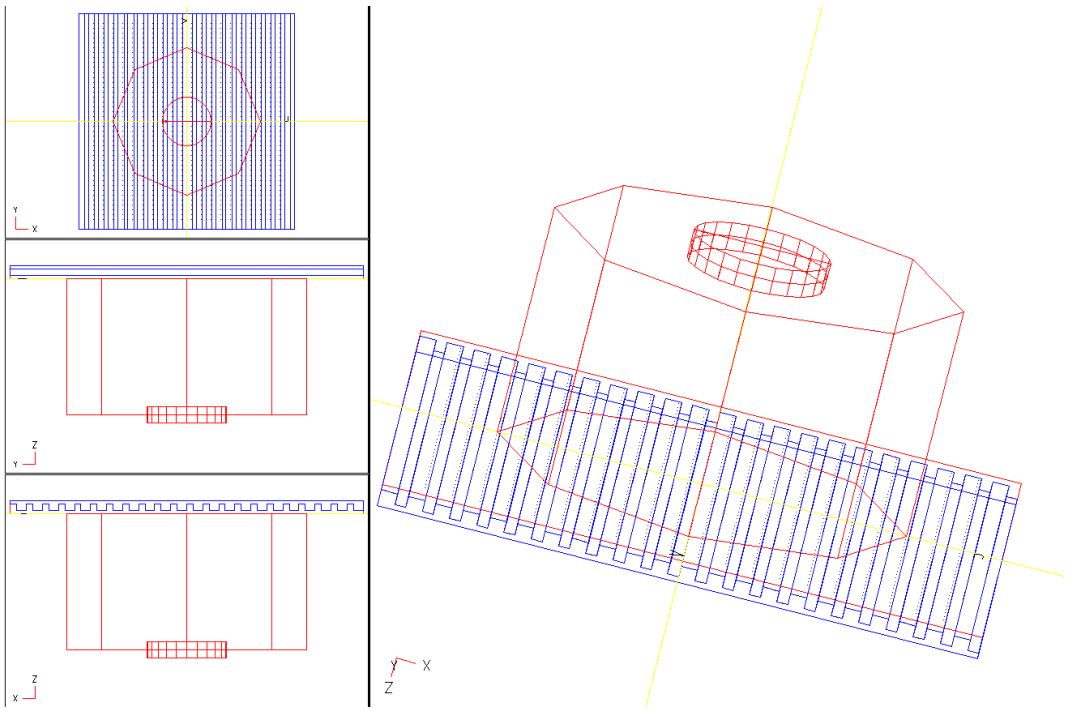

Figure 4.2: Simulation Model

In this model the cylinder on top represents the end of the wave guide. The diameter on the cylinder is the same as the real waveguide, 50mm. In the real system the end of the waveguide is cut with a slight inclination. This is done to get rid of the diffraction from the end of the guide. After a discussion with Jon Anders Aas this is not taken into consideration here.
The eight sided box represents the tank or the radiation chamber. EMDS needs a certain closed volume to be able make its calculations. The side walls and the top is set to be radiation boundaries which implies that no radiation is reflected from the walls and back into the radiation box. This will lead to a sensed field only dependent of the bottom absorber and path loss. To get the right size of the footprint from the waveguide, the diameter of the box had to be calculated. The waveguide has an angle of radiation estimated to be approximately 40° from the symmetry axis [4]. Since the distance from guide to the bottom is 85mm, the diameter of the box is set to be 150mm.
As could be seen from figure 4.2 the absorbent structure is placed underneath the radiation box. In the real system the distance, as mentioned in chapter 1, from the end of the waveguide to the absorbent structure can be up to 150 mm. To keep the calculation volume at a reasonable level this distance is forced to be smaller and is set to 85mm. The polarization can be rotated but for most of the simulations it is set to be normal to the ditches.
EMDS has no direct possibility to do a transformation to the time domain. Since it is impossible to directly track the signal as is propagates towards the bottom absorber, the media in the tank had to be the homogeneous. Simulations with a rising liquid level is therefor not possible. The echo signal would then be the liquid echo, not the wanted echo from the bottom absorber.

4.2 EMDS Simulation

To include phenomenas caused by the bottom structure in the design, extended research was done with the help of Agilent EMDS. Simulations were done on models designed for both LNG and the test liquid paraffin. The simulations were done with a frequency range from 9 to 11 GHz. This should be adequate to represent the bandwidth of the FMCW radar signal used in this gauge system.

4.2.1 LNG

As could be seen from chapter 3 the combination of the the thinnest and thickest absorbent for LNG is in percentage approximately 60/40. Placed in the model described above the magnitude of the E field distribution can be seen in figure 4.3. Here the radiation box is filled with LNG.[2]

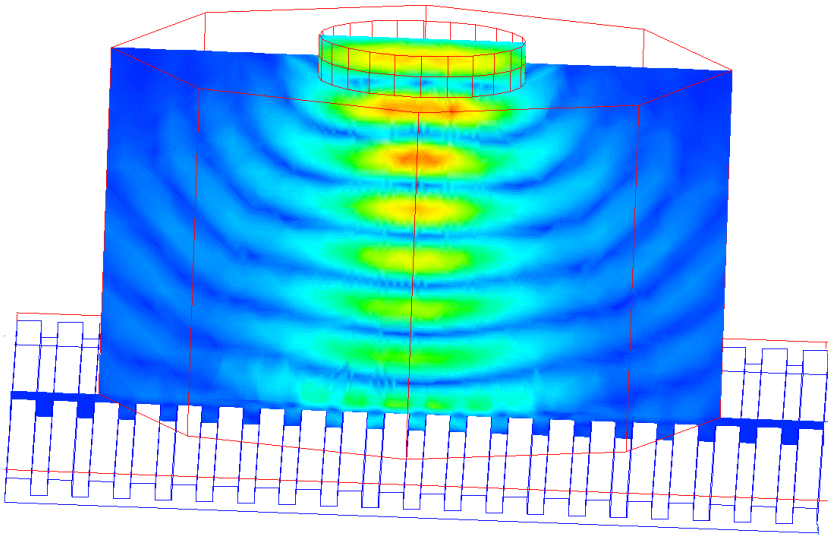

Figure 4.3: E field distribution in the model

[2] A closer look at the field near the bottom can be seen in the appendix.

Type 1

For the bottom absorber to be as easy to install as possible it should be fairly resistant regarding influence on the backscatter due to sideways movement. A metal plate with fine graded structure will serve this purpose. Here each subsection have a total width of 10mm. The structure and the distribution of the absorbent material is shown in figure 4.4. The structure with this distribution will from now on be called type 1.

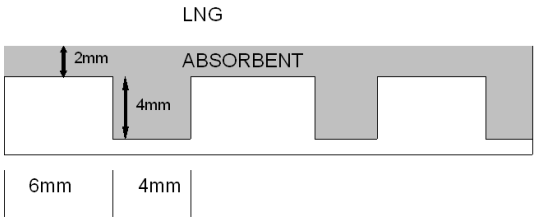

Figure 4.4: Bottom design Type 1 for LNG

The above structure was simulated with a polarization normal to the grooves. As could be seen from figure 4.5 the max attenuation is at approximately 10.5GHz.

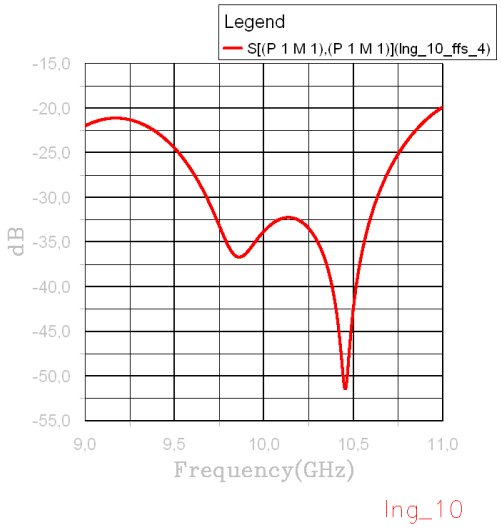

Figure 4.5: S11 parameters for Type 1 bottom absorber designed for LNG

The reason for the deviation from the center frequency is because the different thicknesses influence the total response.

Due to the propagation of the signal in the model additional damping forces is present. To get a more thorough picture of the influence from the bottom absorber a simulation with plane metal plate in the bottom is done. This to get some knowl-

edge about the path loss in the model.

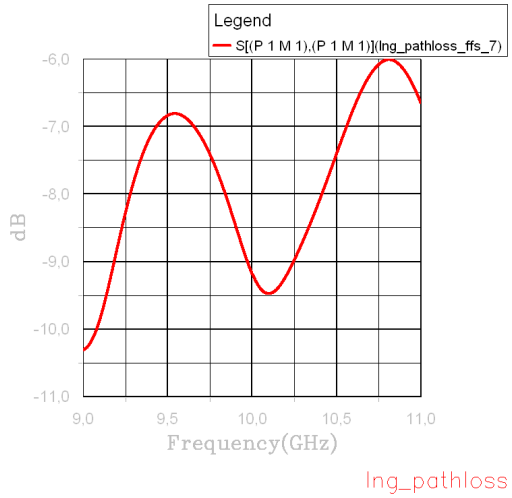

Figure 4.6: Path loss in model with LNG

Type 2

The ditches on the above design is quite small which can be a challenge regarding the cutting and fitting of the RAM. A design with more practical values is shown in the below figure.

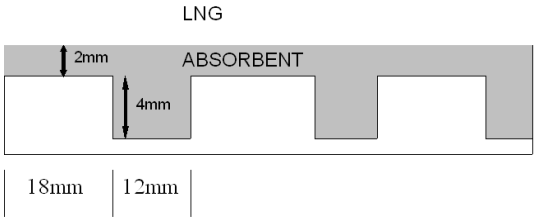

Figure 4.7: Bottom design Type 2 for LNG

The idea and ratio of combination is the same as for type 1 but the total length of each subsection is here 30mm. This leads to a thin part of 18mm and thick part of 12mm.

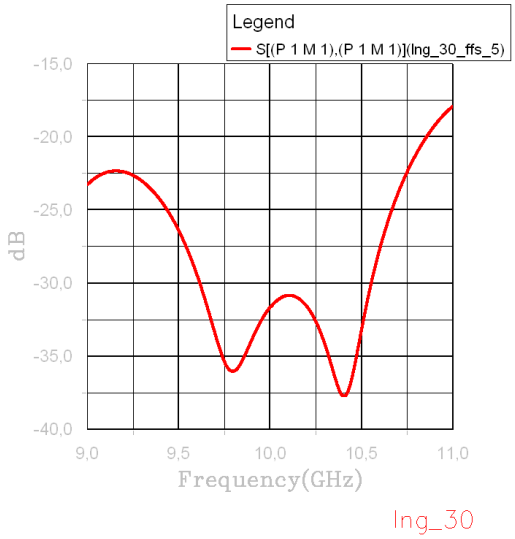

Figure 4.8: S11 parameters for Type 2 bottom absorber designed for LNG

Based on the simulations this type is slightly more wide banded as shown in figure 4.8. On the other hand the type 2 absorbent could be expected to be less adaptive due to sideways movement.

4.2.2 Paraffin

Paraffin has an impedance which is lower than LNG. As could be seen from figure 3.3 on page 19 a thicker absorbent has a lower impedance hence to meet the requirements of a lower total impedance of the bottom absorber more of the thick absorbent should be added.

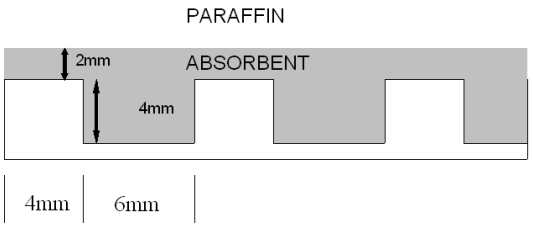

Figure 4.9: Bottom design Type 1 for paraffin

As could be seen in chapter 3 the ideal combination in percentage here is 42.68/57.32 regarding thin/thick part of the absorbent. A more practical ratio would be 40/60 and after simulations this ratio has the same or even better results compared to the ideal ratio (ideal ratio results in appendix). The above figure show the result when

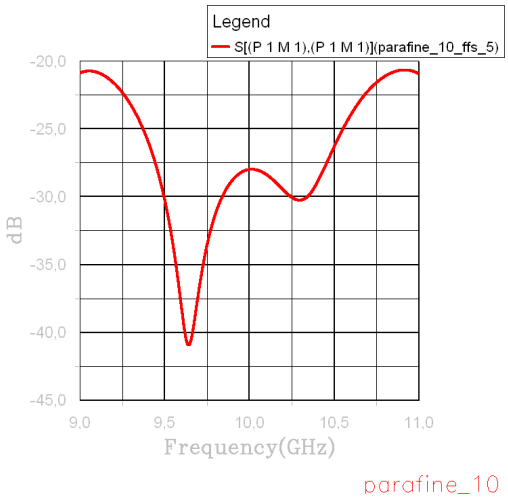

Figure 4.10: S11 parameters for Type 1 bottom absorber designed for paraffin

a 40/60 ratio is used. As for LNG it could be seen that the max attenuation has a deviation from the center frequency due to the interaction between the different thicknesses.

The type 2 results for paraffin gives us slightly lower attenuation than for type 1, but the bandwidth is still reasonable.

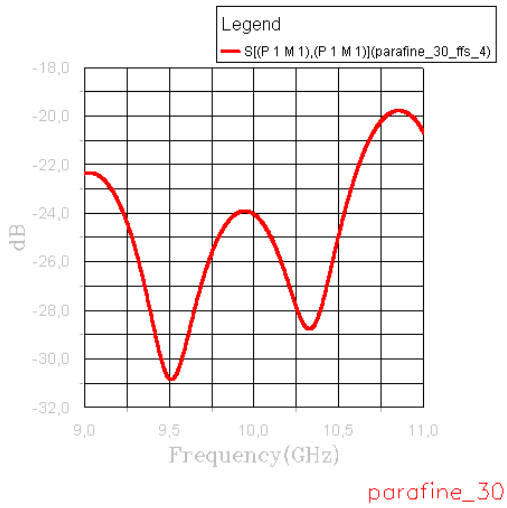

Figure 4.11: S11 parameters for Type 2 bottom absorber designed for paraffin

Since paraffin has a lower impedance than LNG the path loss could be expected to be slightly lower than for LNG. This anticipation corresponds with the below figure.

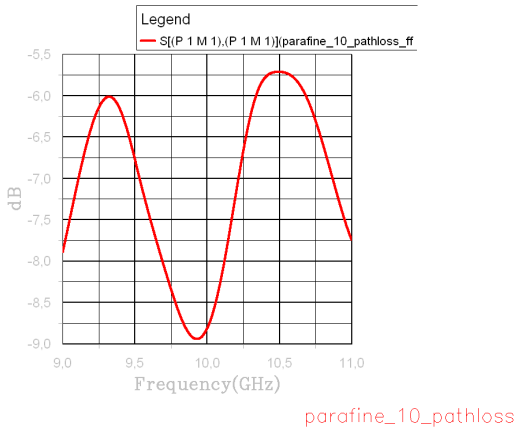

Figure 4.12: Path loss in model with paraffin

4.3 Error analysis

One of the goals of the new design is that it should be easy installable. Deviations from the ideal installation parameters might occur due to error from the craftsmen which are installing the bottom absorber. This means that e.g. an offset from the symmetry line of the waveguide or a deviation in the polarization (E-field not normal to the steps), should not have a negative influence on the attenuation.

To check out possible deviations in the results, simulations with the above mentioned errors are done. Regarding polarization the most interesting case is for small deflection angles, which is more likely than big deflections. In figure 4.13(a) the polarization is turned 15° compared to the polarization normal to the grooves. When

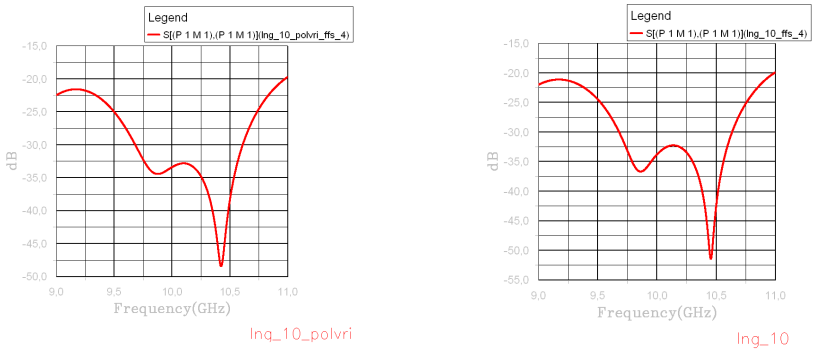

(a) Angeled polarization (b) Normal

Figure 4.13: Polarization test Type1

compared to figure 4.5 on page 27 it can be seen that the attenuation is close to unchanged except for some dB less attenuation at the peak values.

One of the most important issues in the new design is the lack of influence on the backscatter due to sideways movement. In figure 4.14(a) the bottom absorber has an offset of 2mm compared to the earlier simulations.
As could be seen the peak attenuation at 10.4GHz is approximately 10dB stronger, for the rest of the sweep only small deviations is present.

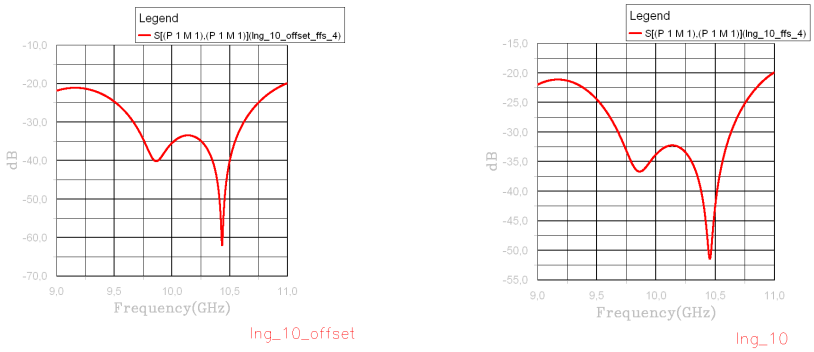

(a) 2mm offset (b) Normal

Figure 4.14: Offset test Type1

The same test as for type1 were done on the type 2 design.

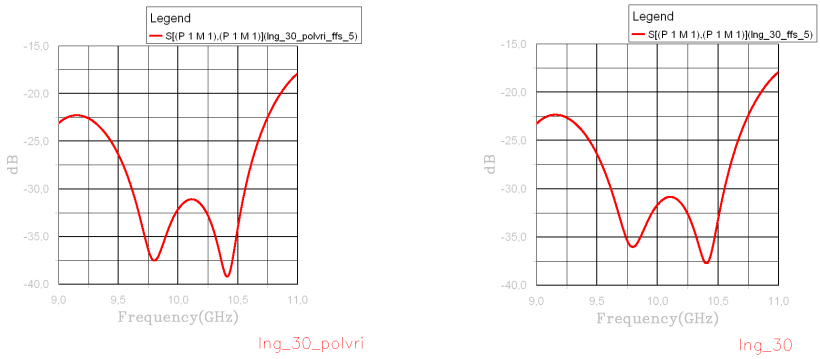

(a) Angeled polarization (b) Normal

Figure 4.15: Polarization test Type2

As could be seen small variation in polarization has more or less no influence on the type 2 absorbent. The attenuation is actually slightly higher with an angeled polarization.

For the type2 absorber an offset of 9 mm was introduced. With this offset the symmetry line of the waveguide is in the middle of highest part of the structure, not at the step as in the preceding simulations.

As expected the backscatter of type 2 is under stronger influence due to sideways

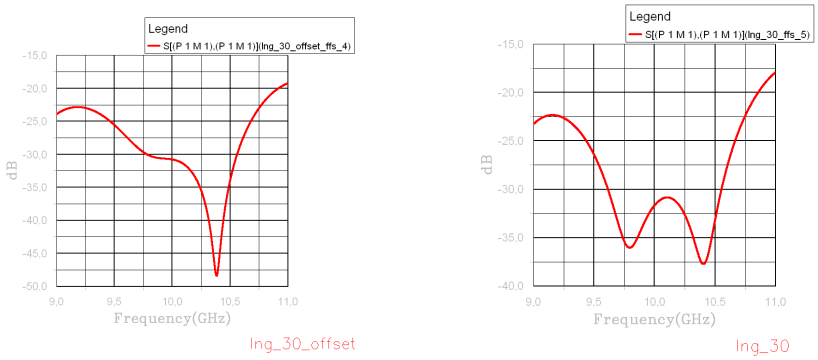

(a) 9mm offset

(b) Normal

Figure 4.16: Offset test Type2

movement. The biggest difference compared with earlier simulations on the type2 absorber is again the attenuation at the resonance of the bottom absorber. Here the attenuation is approximately 10dB stronger. For the rest of the sweep the deviation is smaller, the attenuation is slightly decreased.

Chapter 5

Testing

To check out the design of the bottom absorber, some real life testing has been done. As mentioned earlier the access to LNG test facilities is not possible. These tests were therefore done with paraffin as the reference fluid. The creation and tests were done at the facilities of Kongsberg Maritime Trondheim.

5.1 Creation of Bottom Absorber

The bottom absorber was created on the basis of the calculations and simulations done for paraffin. The steps seen in figure 5.1(a) was milled off a metal plate with a milling machine. Two different bottom absorbers was created, both with the same depth of the ditches and the same ratio of combination but with different width of the subsections.

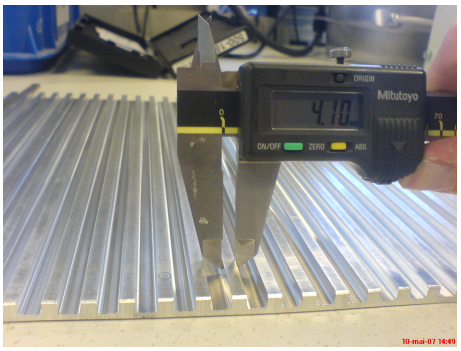

(a) Metal plate with the structure of Type1

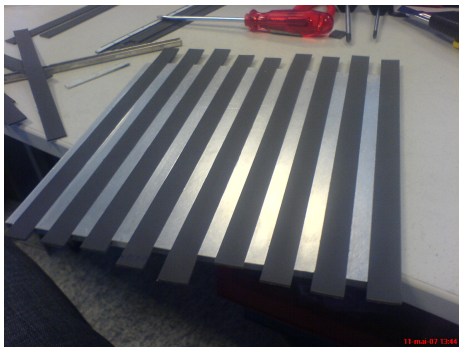

(b) Type2 absorber with filled steps.

In type 1 the total width of each subsection is 10mm, ditch depth of 4mm and width of 6mm. Type 2 has subsections of 30mm, ditch depth of 4mm but with a width of 18mm. The RAM is delivered in plates of 1x1 foot and to make them fit the ditches it was sliced into appropriate size. The RAM was only available with

a thickness of 2mm, so the ditches was filled with two layers on top of each other to reach the hight of 4mm. This leads to a surface shown in figure 5.1(b) , here type2. On top of this surface a new layer of 2mm RAM was placed so that the configuration with thickness of 2 and 6mm was obtained (below picture).

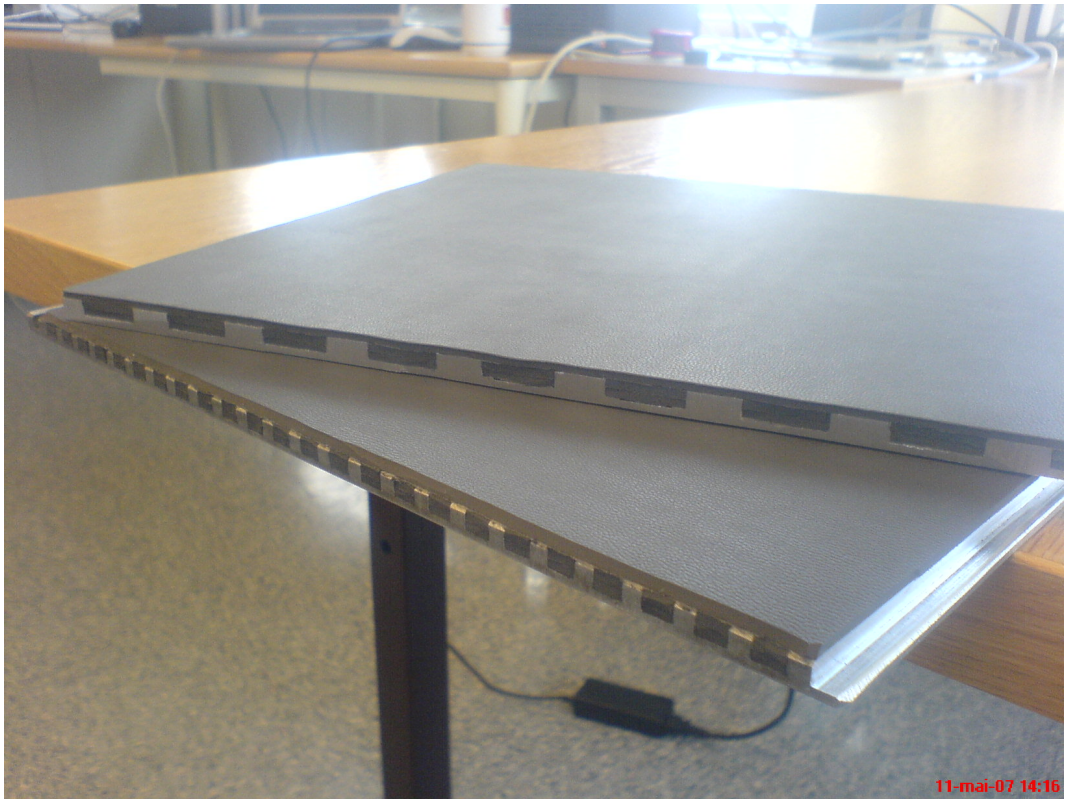

Figure 5.1: The end result. Type2 on top, Type1 at the bottom.

5.2 Measurement set-up

To do the measurements a small scale model of the system was used. The setup used is shown in figures 5.2 to 5.6.

An automatic network analyzer (ANA) from Agilent Technologies was used as a signal unit. It was considered to use the FMCW radar unit, but the possibility to measure and access the measured data in its complex form was found to be an advantage. The ANA was connected to a launcher which launched the signal into the wave guide. The waveguide has an angeled termination as in the real system. This to reduce diffraction phenomena at the guide end. The bottom absorber was placed underneath the waveguide in a small tub so it could be tested against liquid, here paraffin. The height from the waveguide termination to the absorbent plate

Figure 5.2: Measurement set-up

was approximately 85mm, measured from the middle of the angeled cut.

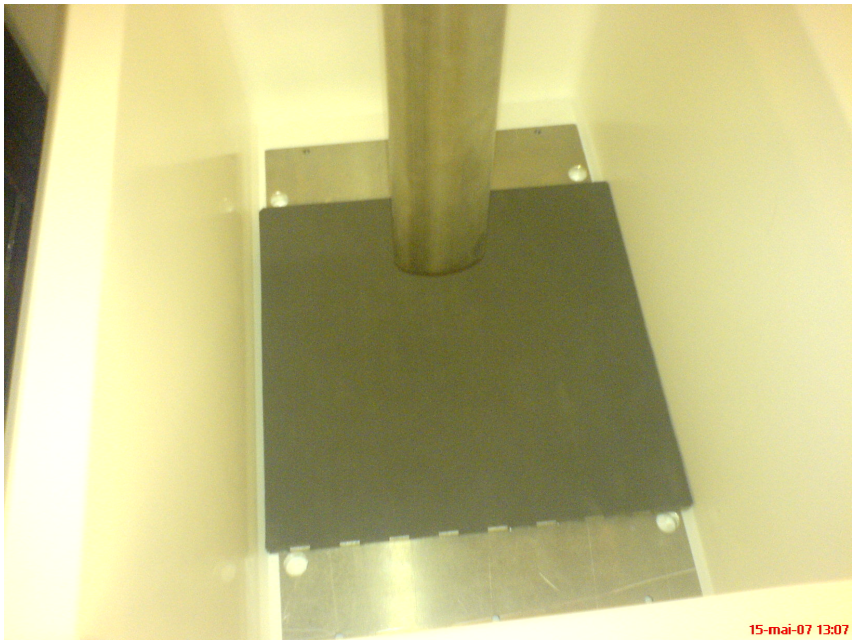

Figure 5.3: Bucket with the bottom absorber placed underneath an angel-cut wave guide

5.3 Measurement against air

To get a correct result the ANA had to be calibrated using a calibration kit in a special procedure. This is essential so that impedance aberrations, lossy contacts and cables is taken under considerations and compensated for.

An investigation prior to the measurement with liquid is of big importance since this will give a characterization of the equipment and serve as reference measurements. Another important possibility is to find the impedance of the bottom absorber "'seen"' by the ANA. These test brings us one step closer to taking a decision if the idea with different thicknesses combinated at a certain ratio is feasible.

5.3.1 The echo signal

The ANA performs a signal sweep over a certain bandwidth. Here a sweep from 9-11GHz with 1601 increments are used. The ANA senses the backscatter and presents the results with the S11 parameters. To find the distance to the object the data is transformed to the time domain with the help of fourier transformation. A normal echo signal can be seen in figure 5.4. The upper signal is the raw data in the

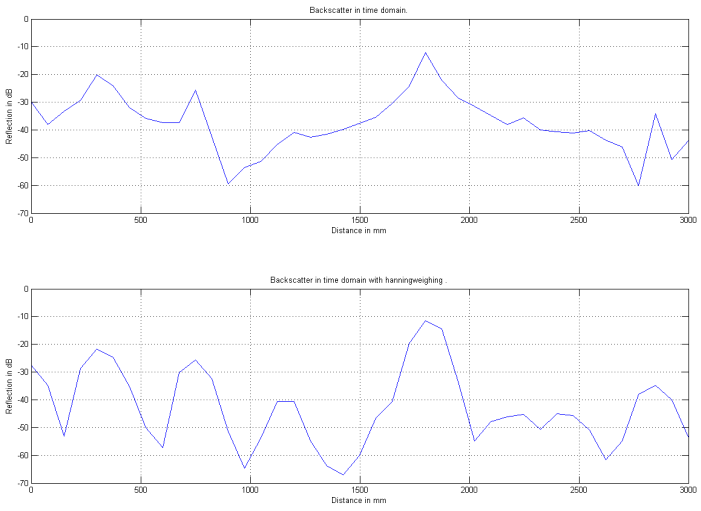

Figure 5.4: Normal reflection from an metal plate in the time domain.

time domain, presented in the most interesting area. The bottom figure is weighted with a Hanning function. Hanning is a known weighting function to suppress side lobes and to handle the sideband effects. As could be seen from the bottom figure

in 5.4 this leads to a concentration of energy in the echoes, the side lobes have less influence on the echo, hence the echoes are easier to distinguish.
Figure 5.4 is the range plot of an echo from a metal surface placed underneath the wave guide. This metal surface is nothing more than the backside of the absorber, which then serves as a perfect range reference.
To smoothen the echo signal, an interpolation of the signal is done by adding a number of zeros to the end of the spectrum. Even though this action increased the effective sample rate, no new information are added [9]. A windowed and interpolated echo signal is shown in figure 5.5. By analyzing the echo signal together with the measurement set-up it is possible to follow the signal through the set-up and determine what the certain echoes represents.

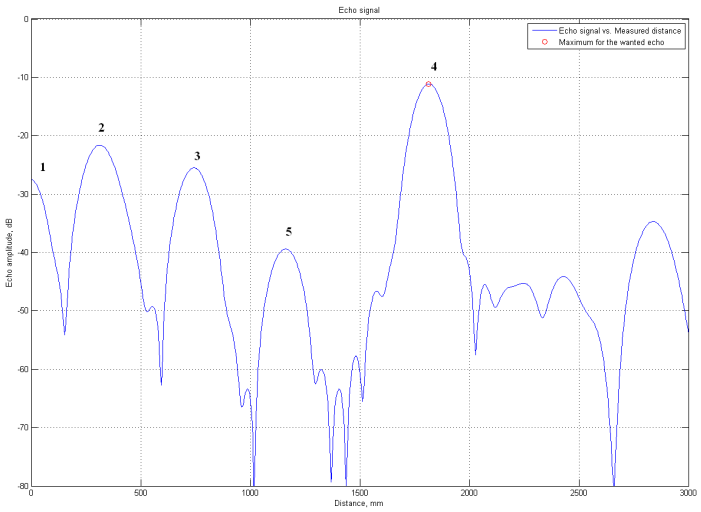

Figure 5.5: Prosessed echo signal for metal plate.

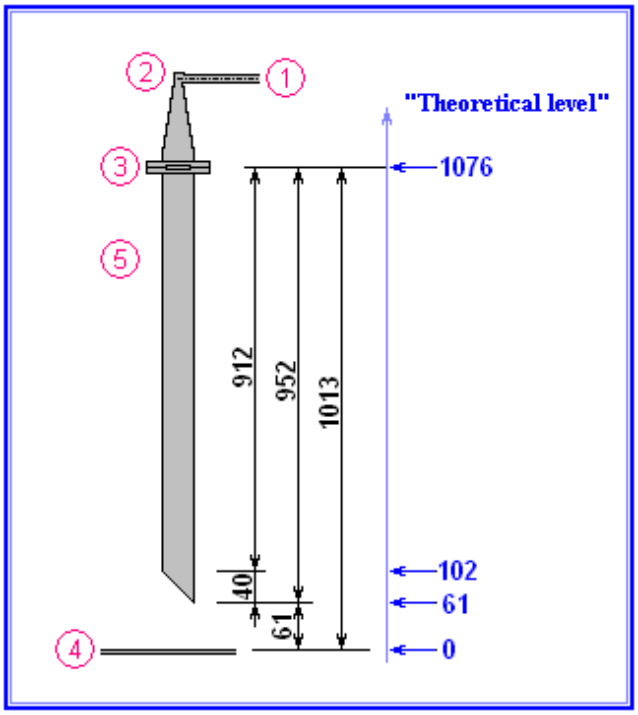

Figure 5.6: Theoretical values for the set-up

The first echo at zero distance is due to mismatch in the connection between the cable from the ANA and the cable of the antenna. The next echo is from the feed on top of the antenna. Echo number 4 represents the sensed object, in this figure a metal plate. This will serve as a reference and the calculated electrical distance from the reference (number 1 in figure 5.6) is 1814mm. Echo number 3 represents the transition from the launcher to the wave-guide. In the setup used there is no galvanic contact in the flange between the feed and the waveguide. The air gap which is present here will produce an echo. The electric distance is measured to be 743mm from the reference plane (echo 1).The measured distance between echo 3 and 4 is then 1071mm.

The propagation speed in the waveguide is lower than in free space. In this waveguide the propagation speed, when filled with air, is approximately 93.6% of the speed of light [1]. The distance from 3 to 4 in figure 5.6 can theorethically be calculated to 1076mm. when the reduced velocity is taken under consideration. This gives a variance of 5mm. The variance can be due to measurements errors, but when using a bandwith of 2GHz 5mm is a bit to much.

To get the theoretical calculated distance to correspond with the measured elec-

[1]With D=50mm, f=10GHz and ϵ_r=1 it could be seen from 2.5 on page 6 that the speed in the waveguide is $V_{guide} = 280.6mmGHz$

trical length, the relative velocity in the waveguide has to be 94.1% of the speed of light. An explanation can be found by taking a closer look at echo number 5. Due to its position this echo could be interpreted as the rebounce of echo number 2 mirrored around echo 3 (same distance from 2 to 3 as 3 to 5), but when taking its echo strength under consideration, which is approximately 33dB to strong for a rebounce of echo 2, this explanation is rejected. Due to the air gap between the launcher and the waveguide it is highly possible that a higher order mode is created and echo number 5 is a double transit of such a mode. If this is present, a transformation of only 2% of the siganl energy would be adeuqate. Half of this energy is propagating back towards the ANA, but this energy would be reflected in the cone of the launcher (only fundametal mode will pass) and propagate back to the airgap. In the airgap 2% of the energy of a higher order mode will then convert back to the fundamental mode. This echo can be described as echo 5.
Regarding the distance error of echo 3 the explanation can be exactly this possibility of energy conversion in the air gap. With such a conversion there is often a local energy storage around the step which would have an influence on both the group time delay and the reflected and transmitted signal in fundamental mode.

5.3.2 Bottom absorber impedance calculations

The purpose of the bottom absorber is merely to reduce the backscatter from underneath the waveguide. For the absorber to work, the energy has to be able to pass through the interface between the liquid and absorbent. As explained in previous chapters, for the energy to be transmitted into the RAM and not be reflected at the interface, the impedance of the medias on each side of the interface have to be equal. The test liquid used has the impedance $Z_{par} = 251\Omega$, hence the desired impedance "'seen"' on the surface of the absorber is $Z_{abs} = 251\Omega$.

The whole system can be seen as a parallel to an arbitrary two-port with scattering matrix [S] as shown in the below figure.

A series expansion can be done and has the form [7]:

$$\Gamma_{in} = S_{11} + \frac{S_{21}^2 \cdot \Gamma}{1 - S_{22} \cdot \Gamma} \tag{5.1}$$

When transformed to the time domain, unwanted echoes can be filtrated. The parameter which tells us how the bottom absorber influence the signal (S_{21}) can then easily be distinguished.

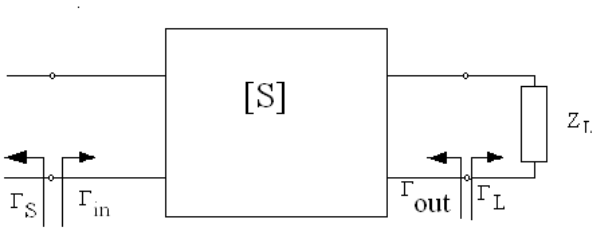

Figure 5.7: Two port.

As mentioned the measurements done with a metal surface at the bottom serves as a reference. The metal surface is regarded as a short-circuit, hence the reflection is a known coefficient, $\Gamma_{short} = -1$ [7]. In this case this is not the entire truth because Γ_{short} will contain an additional damping factor and a phase shift due to the propagation of the signal. With reference to equation 2.13 to 2.16 on page 8 the reflection coefficient for the metal surface can be expressed as:

$$\Gamma_{metal} = \Gamma_{short} \cdot e^{-\alpha 2R} e^{-j2kR} \tag{5.2}$$

When doing these measurements on the bottom absorber, the reflection coefficient Γ_{abs} will contain the same parameters as for Γ_{metal}. Since the propagation path is the same as for metal and Γ_{short} is known, the true reflection coefficient for the bottom absorber "'seen"' by the ANA can be found:

$$\Gamma_{abs} = \frac{\Gamma_{absTrue} \cdot e^{-\alpha 2R} e^{-j2kR}}{\Gamma_{short} \cdot e^{-\alpha 2R} e^{-j2kR}} = \frac{\Gamma_{absTrue}}{-1} = \Gamma_{-absTrue} \tag{5.3}$$

Since the media above the surface is air, which is characterized by the free space impedance $Z_{air} = 377\Omega$, the impedance of the absorber "'seen"' by the ANA can now be calculated using equation 2.11 on page 7.

$$\Gamma_{absTrue} = \frac{Z_{abs} - Z_{air}}{Z_{abs} + Z_{air}} \Longrightarrow Z_{abs} = 377 \cdot \frac{1 - \Gamma_{absTrue}}{1 + \Gamma_{absTrue}} \tag{5.4}$$

Γ_{abs} is obtained by doing measurements with the absorbent placed in the bottom of the tub, without liquid.
It could be seen from figure 5.8 that type1 absorber has a lower impedance than

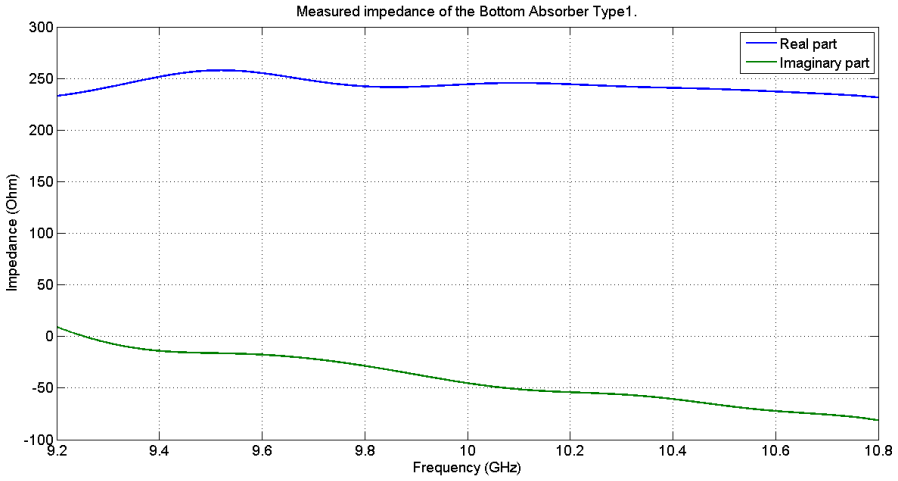

(a) Type1

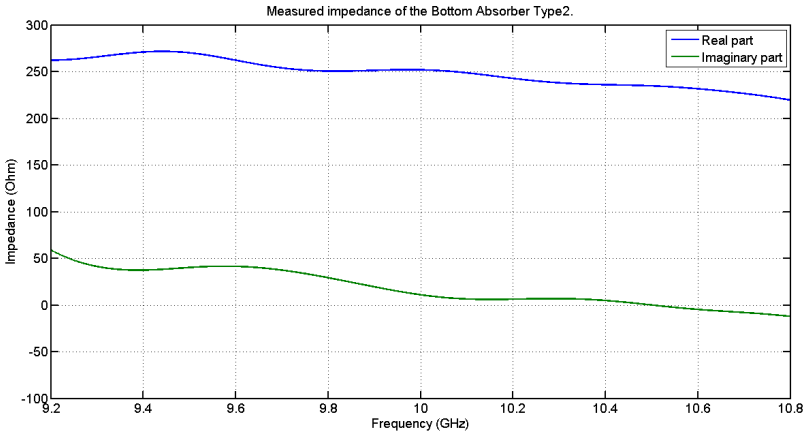

(b) Type2

Figure 5.8: Input impedance for the bottom absorber

paraffin. At center frequency the real part is 244.5Ω and imaginary component -45Ω which makes the bottom absorber capacitive.

Type 2 has a higher input impedance, real part of 252Ω and an imaginary part of 11Ω which implies a slightly inductive bottom absorber.

A positive result seen form figure 5.8 is that the absorber is quite frequency independent. One way to get an idea about the frequency dependence is by taking a look at the Q-factor [18]. In this case the the Q- factor is given by

$$Q = \frac{f_0}{2} \cdot \frac{\frac{\partial}{\partial f} Im}{Re} \mid_{f_0} \tag{5.5}$$

With the help of the above figure the Q-factors is found to be:

$$Type1: \ Q = \frac{10}{2} \cdot \frac{(5+75)/(10.8-9.2)}{244.5} = 1.02$$
$$Type2: \ Q = \frac{10}{2} \cdot \frac{(55+5)/(10.8-9.2)}{252} = 0.74$$

With Q value of about 1 and lower it can be said that the bottom absorber is quite frequency independent and with a wider bandwidth. It could be seen that the impedance tends to fall when the frequency increases. This is due to the fact that the radiation angle decreases when the frequency increases, the radiated energy will be more concentrated which again will produce a slight increase in the reflection.

5.4 Measurements with paraffin

To check out the designed bottom absorber a series of test with paraffin were done. Paraffin was pumped into the tub shown in figure 5.3 on page 37 at certain intervals. This amount is in the first coloum of the table, referred to as setting. To determine the ullage and hence also the measured level, the reference measurement was used. The table below summarize the results.

	Measured			
Setting (mm)	Level (mm)	Echo strength (dB)	Difference (mm)	remarks
Reference	0.0	-11.0307	0.0	
0	11.0783	-23.9617	11.0783	
3	0.2887	-23.1774	-2.7113	
10	14.2354	-23.3714	4.2354	
30	30.9840	-21.1340	0.9840	
50	52.5477	-21.4787	2.5477	
70	58.4500	-17.6310	-11.5500	
80	72.5747	-16.9876	-7.4253	
90	86.9577	-16.1084	-3.0423	
100	101.5276	-15.5358	1.5276	outlet covered
150	144.8572	-15.2820	-5.1428	
200	197.1337	-15.3028	-2.8663	

Table 5.1: Measurements with paraffin

As could be seen from figure 5.9 the echo strength tends to stabilize when the liquid is in the waveguide.
The expected reflection air - paraffin in the waveguide is -13.2dB[2]. The values measured are influenced by attenuation in the system, when inside the waveguide the attenuation from the pipe itself is also a part of the measured value. A measurement with a metal plug covering the outlet lead to an attenuation in the waveguide of approximately 1.6dB. The real echo produced at the interface air - paraffin in the waveguide can be calculated to be -15.3dB + 1.6dB = -13.7dB. The echo strength produced at the interface is 0.5dB lower than expected. This can be an indication that the permittivity of the paraffin used is lower than 2.25 (lower permittivity gives higher impedance –> impedance closer to air leads to a lower reflection.)

[2]Equation 2.6 gives us $\Gamma = \frac{258.3-402.4}{258.3+402.4}$ = -0.218.

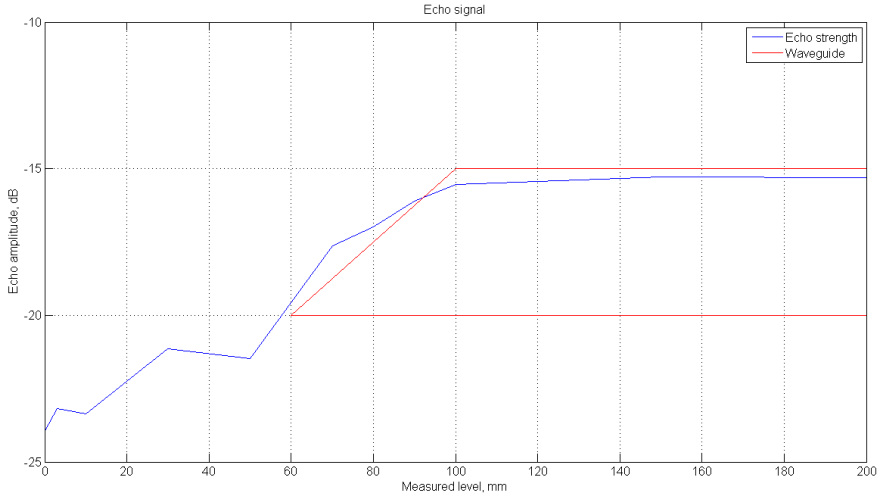

Figure 5.9: Echo strength at different levels.

Some uncertainty can be expected regarding the real level of fluid since it was measured with an inch rule and the human eye.

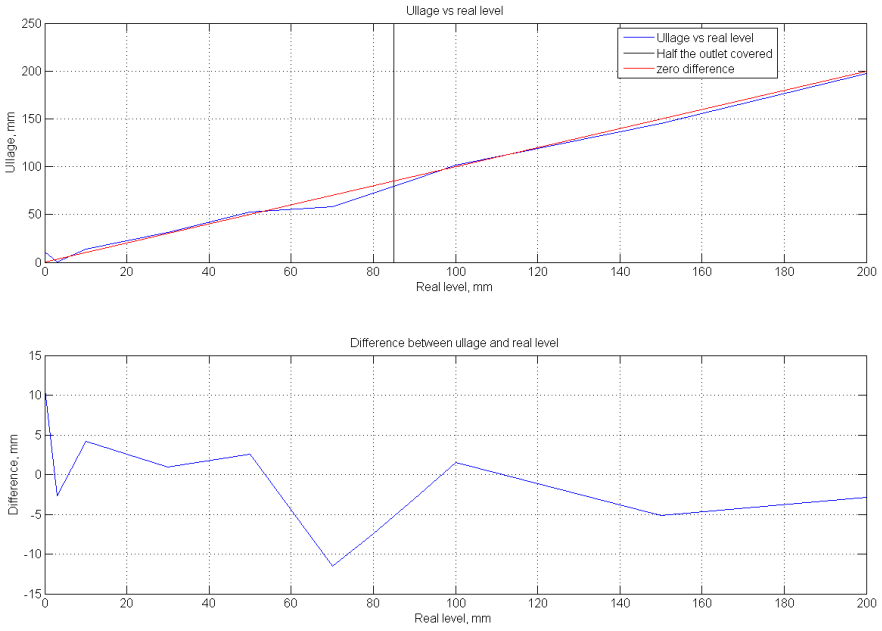

Figure 5.10: Difference plot

With a level of 85 mm the liquid is covering half of the waveguide opening. From the above figure it could be seen that as long as the liquid is inside the waveguide

the sat level corresponds to the measured level. Only small deviations is present for the whole test series, mostly all of the test are inside a $\pm$ 5 mm certainty. One big deviation is at approximately 70mm when the measured level is 11.5mm below the real level. The echo strength produced at this level is normal compared to the others hence this deviation might caused by reading error.
Another deviation is at zero level, when no liquid is on top of the bottom absorber. This is a known phenomena when coming to resonance structures. In this case the bottom seems to closer than the true distance. With an impedance lower (paraffin) than the reference impedance (air), there will be a lift in the phase-frequency characteristic which is the component the distance measurements are based upon.

When reaching a certain level of liquid in the tub the echo from the bottom absorber starts to separate from the much stronger liquid echo. In figure 5.11 it is possible to sort out the bottom echo which have an echo strength of approximately -36.1dB.

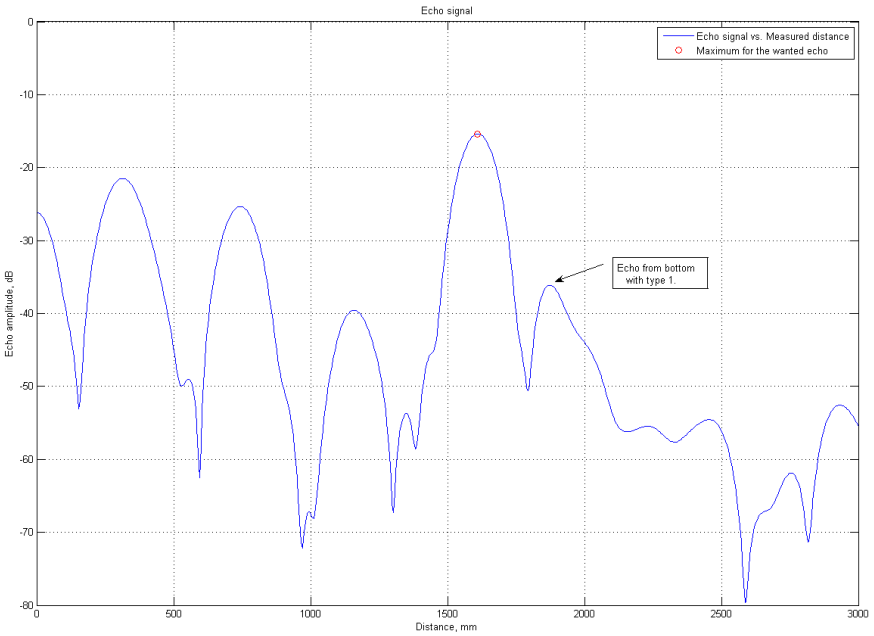

Figure 5.11: Echo from subnerged bottom absorber

With the expected permittivity of paraffin is 2.25 (index of refraction approx 1.5) it is legal to assume that the echo is 3.5dB higher than surrounded by air. The path loss for the setup-up in air (from the measurement with the metal plate) is found to be -11.1dB. The isolated echo strength from the bottom absorber can then

be presented as -36.1 -3.5 + 11.1 = -28.5dB. The distance from the the liquid and the bottom absorber in this example is 200mm. The echo separation should then be approximately 300mm due to the index of refraction of paraffin. The distance is measured to be approximately 263mm. This is a bit smaller than wanted which implies that this echo location is under strong influence of the much stronger liquid echo.

When using the measurement where the level is 150mm the measured distance is approximately 223, which when divided by 1.5 gives us 149mm. This is in accordance with the real level and the signal strength is then -37.5dB. This implies -37.5 -3.5 + 11.1 = -29.9dB.

Based on these rough calculations the actual echo from the bottom absorber seems to be around -30db which means that just 0.1% of the energy that reaches the bottom absorber is reflected.

Chapter 6

Discussion

In this section some of the results and methods are discussed in order to validate the ideas and trade-offs.

6.1 Thickness

When choosing the thickness in section 3.2 on page 17 it is referred to better bandwidth when choosing a combination of thickness of 2mm and 6mm. These statements have been experienced in the pre-study. If the model with the absorbing material backed with a metal plate is transformed to a circuit equivalent one explanation of this phenomena can be found. At thickness 1 and 3 we have a trailing edge (3.3) which will give us a resonant circuit in parallel. Thickness 2 is located on a leading edge which will give a series resonance circuit.

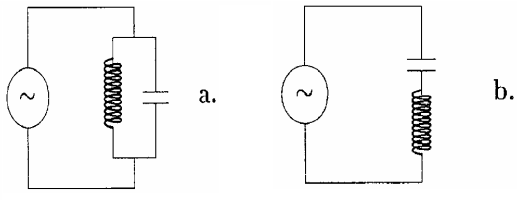

Figure 6.1: Resonant circuits

A combination of two parallel resonators gives a higher bandwidth than one in series and one in parallel.

6.2 Permittivity of paraffin

It can be seen from the test results in section 5.4 that the echo from the paraffin tends to stabilize at approximately -15.3dB. 1.6dB is due to loss in the waveguide (ref measurements with metal plug), hence the real echo from the fluid is -13.7dB. By using equation 2.11 on page 7 with the wave impedance in the waveguide and the measured reflection, the impedance of paraffin can be found to be approximately Z_{par}=265. This leads to a permittivity of about 2.

6.3 Bottom absorber calculations

The starting point regarding the combination ratio of different thicknesses are stated in Chapter 3, equation 3.4 on page 19. Here the wanted reflection is 0 which implies that the impedance of the reference media is the same as the designed bottom absorber.

In section 5.3.2 on page 41 the input impedance of the bottom absorber designed for paraffin was found using air as a reference medium. Air and the bottom absorber have different impedance hence there will be a reflection at the interface. To do tests with the liquid which the bottom absorber is designed for can some times be quite challenging. The use of air as a reference medium would be very useful and practical, so a possible deviation is checked out.

If the reference medium is different from medium which the bottom absorber is designed for equation 3.4 on page 19 can be written as:

$$\Gamma_1 \cdot k_2 + (1 - k_2) \cdot \Gamma_2 = \frac{Z_{bottomAbsorber} - Z_{referenceMedium}}{Z_{bottomAbsorber} + Z_{referenceMedium}} \tag{6.1}$$

If the the bottom absorber is referred to as Z_L and the reference medium is air the above equation can be written as:

$$k_2 \cdot \frac{R1 - Z_0}{R1 + Z_0} + (1 - k_2) \cdot \frac{R3 - Z_0}{R3 + Z_0} = \frac{Z_L - Z_0}{Z_L + Z_0} \tag{6.2}$$

$$\Downarrow$$

$$Z_L = Z_0 \cdot \frac{1 + (k_2 \cdot \frac{R1 - Z_0}{R1 + Z_0} + (1 - k_2) \cdot \frac{R3 - Z_0}{R3 + Z_0})}{1 - (k_2 \cdot \frac{R1 - Z_0}{R1 + Z_0} + (1 - k_2) \cdot \frac{R3 - Z_0}{R3 + Z_0})} \tag{6.3}$$

where R1 and R3 is the real part of the impedance with thickness 1 and 3 ref. table 3.2 on page 18.

When comparing these ways of testing the input impedance the difference is al-

most neglectable. In figure 6.3 the input impedance vs the ratio of combination is plotted with both air and paraffin as reference medium. The black circles on the

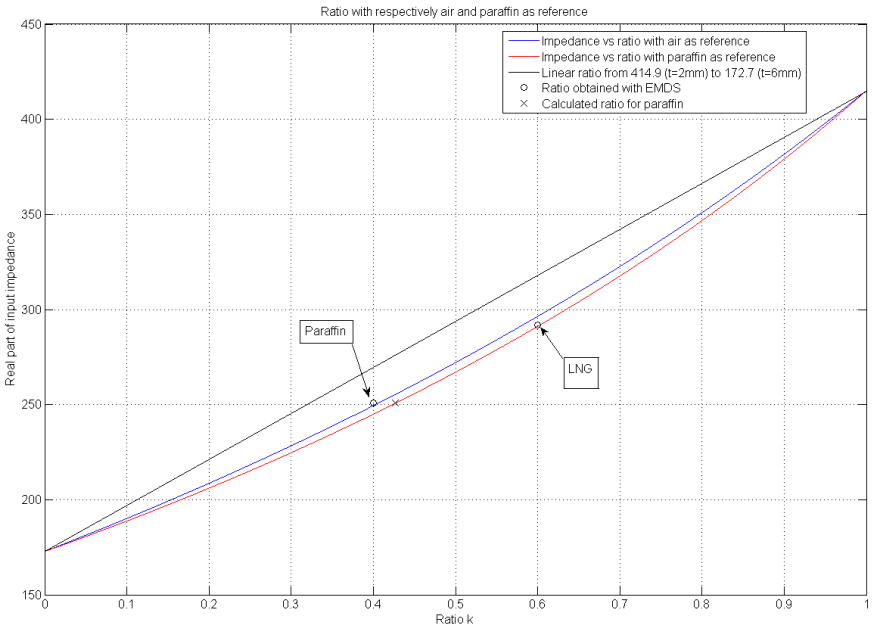

Figure 6.2: Validation of air measurements

above figure points out the ratio and the corresponding input impedance obtained in EMDS. As could be seen the circle for paraffin (Z = 251Ω) and LNG (Z = 292Ω) is practically speaking on the line which represents air as a reference medium.
This realization leads to a much easier way of testing the bottom absorber.

6.4 Input impedance of the bottom absorber

The input impedance found in section 5.3.2 on page 41 has for both types just small deviations from the wanted value of 251Ω. The type 1 design has a slightly lower impedance than wanted. In order to increase the input impedance for the bottom absorber designed for paraffin the section of the RAM with thickness of 2mm has to be increased. The bottom absorber was simulated with a ratio 40/60 despite that the calculations gave a ratio of 42.68/57.32. The ratio 40/60 was chosen as a "'practical ratio"' since simulations with the calculated ratio had more or less the same results.
From the discoveries in the test this can indicate that the calculated ratio is a better starting point.

On both the type 1 and the type 2 design an imaginary part was sensed. The biggest deflections where found in the type 1 design which had an imaginary part of $Z_{imag} = -45\Omega$. This implies a capacitive behavior. One explanation can be the design of the metal plate and its grooves. Capasativity implies storage of energy. When taking a look at the simulation of the step there is clearly a congestion of energy around the step and thus an explanation of the capasative behavior. When increasing the sizes as in type 2 there is longer distances between the steps. With this increased distance the energy congestion does not influence the total result in the same way.

When trying analyze the influence of the capasative / inductive part regarding matching, a comparison with the standing wave ratio (SWR) is a useful start. This can be done by plotting the backscatter of both bottom absorbers together with a circle representating the SWR. This plot can be done in the Smith chart or in a rectangular plot as here. A SWR = 1.2 corresponds to a reflection of approximately -21dB. To get the right size of the SWR circle its radius and center has to be found.

$$SWR_{center} = \frac{251(s + 1/s)}{2} = \frac{251(1.2 + 1/1.2)}{2} = 255.2$$
$$SWR_{rad} = \frac{251(s - 1/s)}{2} = \frac{251(1.2 - 1/1.2)}{2} = 46.0$$

This together with the complex backscatter from measurements on the type 1 and 2 bottom absorber creates the figure as shown in 6.4.

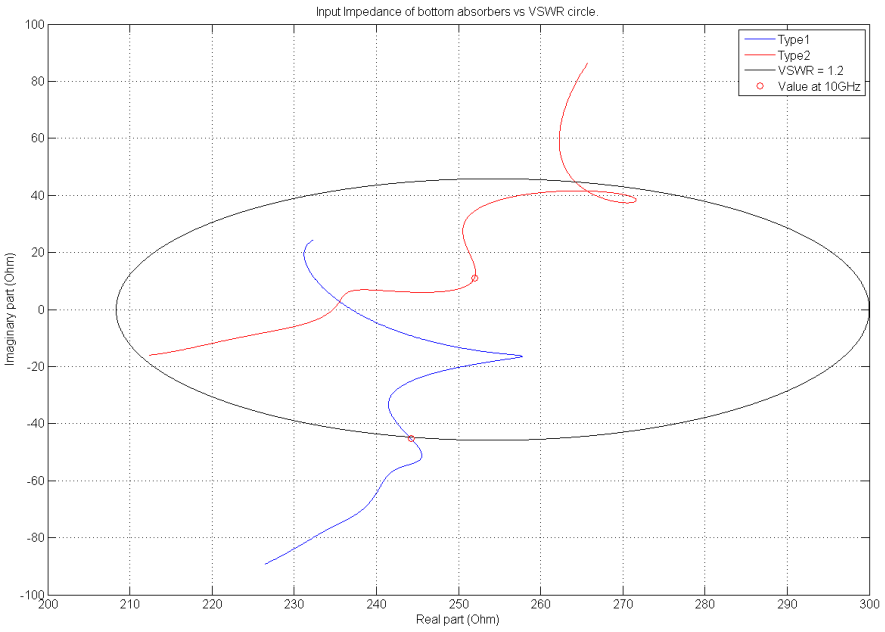

Figure 6.3: Input impedance vs SWR

Chapter 7

Conclusion

The idea as mentioned in the start of this paper was to design a non symetric, easy installable bottom absorber. To get the absorber to serve its purpose it should be designed to match a reference medium. Since testing with LNG is unpractical, a bottom absorber design to match paraffin with an impedance of 251 Ω was created.

Due to the test results it can be said that the design criteria is within range. Only a small correction in the ratio of the type 1 absorber will lead to a perfect match to paraffin. In the test with paraffin the reflection from the bottom absorber was calculated to be -30dB. This means that only 0.1% of the incident energy is reflected. The difference in strength between the echo from paraffin and the echo from the bottom absorber is 16dB. This means that the echo from paraffin is something like 40 times as strong and should be possible to detect.

From simulations and during the tests it was found that the design was adaptive regarding sideways movement and small distortions in polarization. This will ease the problems concerning installation problems.

During the analysis it was also discovered that doing test with air as a reference, though the bottom absorber is designed to match other impedances, is a valid way of doing impedance tests. Only small deviations were found.

The end result of the design is of such a character that Kongsberg Maritime is willing to realize / adapt the idea and use it in their commercial level gauge system.

7.1 Future Work

As mentioned the phenomenas near the bottom absorber is quite complex. The imaginary part of the reflection obtained from the bottom absorber varied from type 1 to type 2. A study of the diffraction phenomenas around the steps and the interaction between the subsections will probably give some answers regarding this.

One way of coming closer to an imaginary part equal to zero could be by varying the total size of each subsection. 10mm for type 1 and 30mm for type 2 are investigated. Maybe a subsection with total width of 20mm would have a imaginary part closer to zero. The simulated responce is shown in the appendix.

At the end of my study a way of extracting data from the simulation programme was found. It is then possible to track the signal with the help of analysis in e.g Matlab. This makes it possible to design simulation models closer to the real system.

References

[1] David K. Cheng. *Field and Wave Electromagnetics*. Addison Wesley, second edition, 1992. ISBN 0-201-12819-5.

[2] John F.; Tuley Michael T. Knott, Eugene F.; Shaeffer. *Radar Cross Section (2nd edition)*.

[3] Colm Mansfield, Michael; O'Sullivan. *Understanding Physics*. John Wiley & Sons, 1999.

[4] Personal communication with Øyvind Jensen, 2007.

[5] Prof. Ali M. Niknejad. Wave propagation in lossy media and poyntingŠs theorem. *University of California, Berkeley*, 2004. URL `http://rfic.eecs.berkeley.edu/ niknejad/ee117/pdf/lecture21.pdf`.

[6] Gorur G. Raju. *Dielectrics in electric fields*. Marcel Dekker, Inc., 2003. ISBN 0-8247-0864-4.

[7] David M. Pozar. *Microwave and RF Wireless Systems*. John Wiley & Sons, 2001. ISBN 0-471-32282-2.

[8] Jerome L. Altman. *Microwave Circuits*. D. Van Nostrand Company, 1964.

[9] Byron Edde. *Radar - Principles, Technology, Applications*. Prentice Hall PTR, 1993.

[10] Charles Elachi. *Introduction to the physics and techniques of remote sensing*. John Wiley & Sons, 1987.

[11] Constantine A. Balanis. *Antenna Theory*. Wiley-Interscience, third edition, 2005. ISBN 0-471-66782-X.

[12] K.J. Vinoy and R.M Jha. *Radar Absorbing Materials: from theory to design and characterization*. Kluwer Academic Publishers, first edition, 1996. ISBN 0-7923-9753-3.

[13] Kenneth Sivertsvik. Wavelet as an analytical tool in a FMCW Radar. Master's thesis, NTNU, 2003.

[14] Øyvind Jensen. Internal presentation of FMCW principles. *Kongsberg Maritime*.

[15] Samuel 0. Piper. Homodyne fmcw radar range resolution effects with sinusoidal nonlinearities in the frequency sweep. 1995. URL http://ieeexplore.ieee.org/iel3/3929/11378/00522609.pdf?arnumber=522609.

[16] Harald Bjerkan. Performance characteristics of resonant absorbers, dällenbach layers. Internal document Kongsberg Maritime.

[17] Arne Helge Andersen. Theoretical / practical study of equipment for reducing radar backscatter. Project report, Department of Electronics and Telecommunications, NTNU, 2006.

[18] J. F. Borges da Silva J. A. Brandâo Faria. Q-factor and bandwidth estimation of sharp resonant phenomena in transmission line systems with grounding points. *Electrical Engineering (Archiv fur Elektrotechnik)*, 1989. URL http://www.springerlink.com/content/j41135387811214k/fulltext.pdf.

Appendix A

Appendix

A.1 Derivation of Input Impedance [6,p299-300].

Free space wave number: $k_o = w\sqrt{\mu_0\epsilon_0}$

The intrinsic impedance Z of the material:

$$Z = Z_0\sqrt{\mu_r/\epsilon_r}$$

where

$$Z_0 = \sqrt{\mu_0/\epsilon_0}$$

For a flat metallic surface coated with a layer of dielectic material with thickness d, the normalized input impedance η is given by

$$\eta = \sqrt{\mu_r\epsilon_r}tanh(jk_0d\sqrt{\epsilon_r\mu_r})$$

When not normalized and combined with the intrinsic impedance and the free-space wave number we get

$$\begin{aligned} Z &= \sqrt{\mu_0/\epsilon_0}\sqrt{\mu_r/\epsilon_r} \\ &= \sqrt{\mu/\epsilon} \end{aligned}$$

$$\begin{aligned} Z_i &= \sqrt{\mu\epsilon}tanh(jdw\sqrt{\mu_0\epsilon_0}\sqrt{\epsilon_r\mu_r}) \\ &= Ztanh(jwd\sqrt{\epsilon\mu}) \end{aligned}$$

A.2 Simulation

A.2.1 Currents in bottom absorber

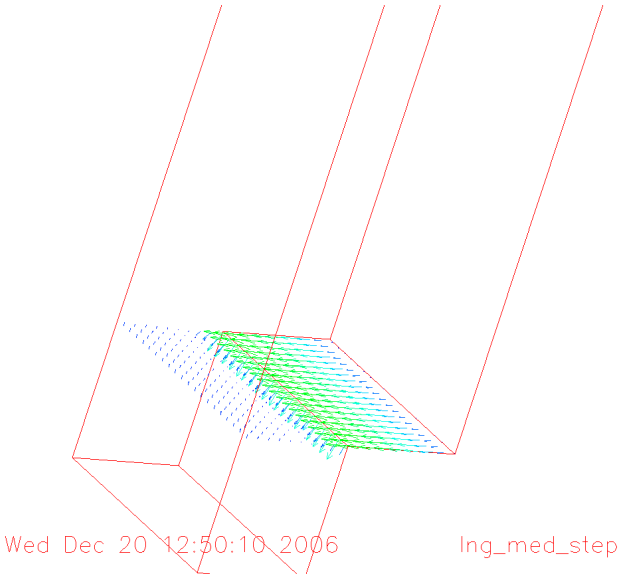

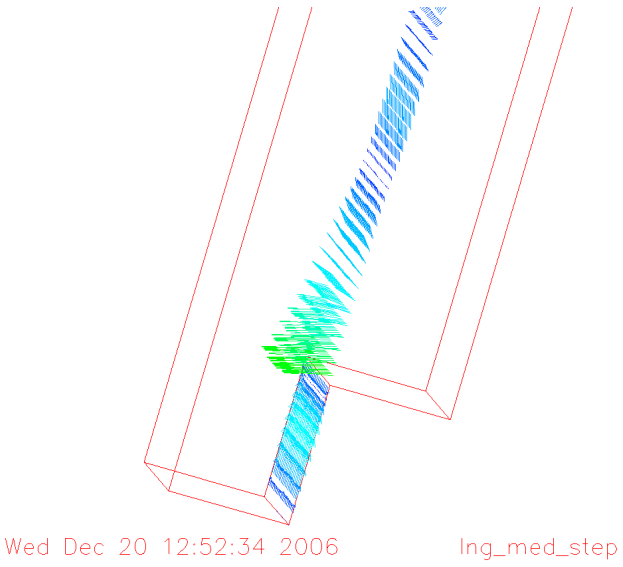

A.2.2 E-field near bottom in simulation model

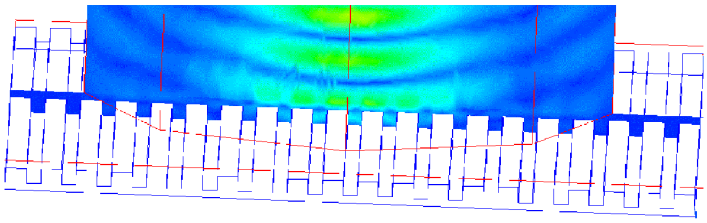

Figure A.1: E-field near bottom

A.2.3 S11 for paraffin with ideal ratio

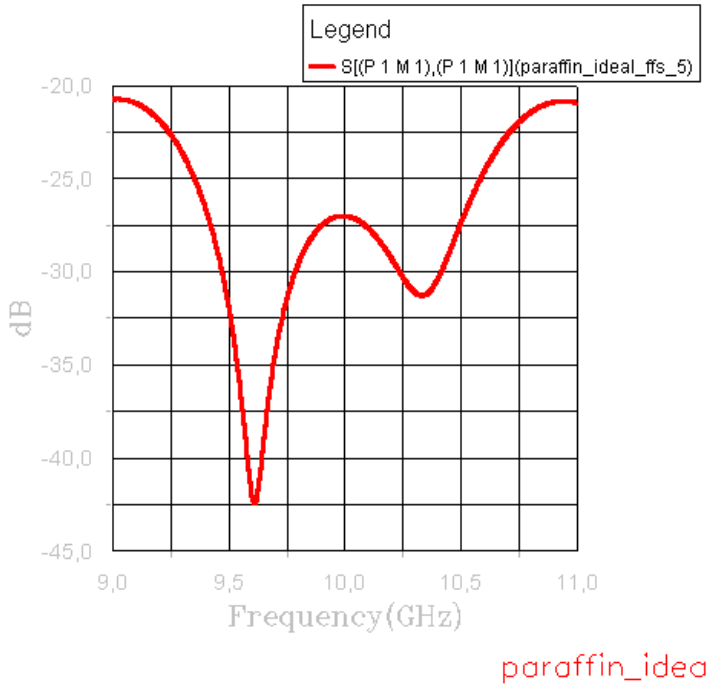

Figure A.2: S11 for paraffin with ideal ratio

A.2.4 S11 for paraffin subsection-width = 20mm

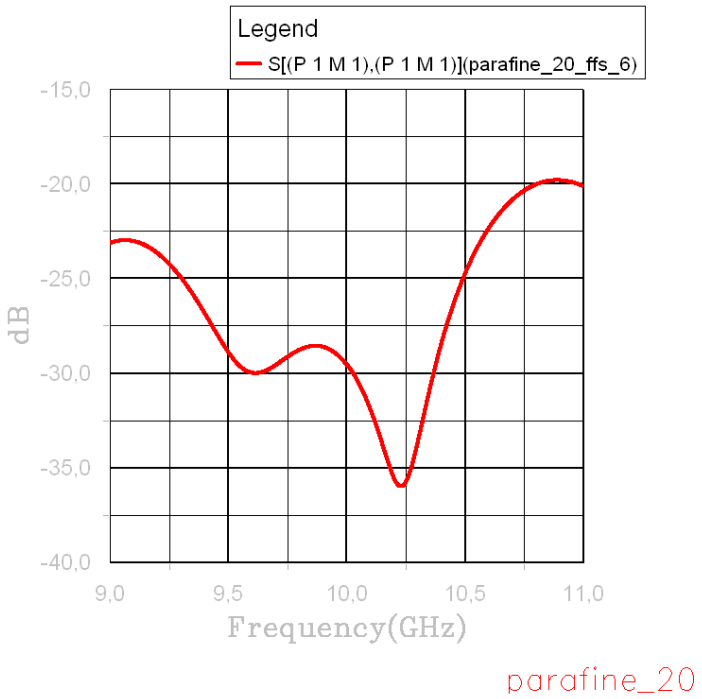

Figure A.3: Width of subsection = 20mm

A.3 Matlab code

A.3.1 Input Impedance of RAM

```
1   clear all;
2
3
4   %% Constants
5   Er = 10.5 - j*0.3;
6   Ur = 1.2-j*0.5;                    %permability
7   E0=8.8541878176e-12;               %permittivity of vacum
8   U0=4*pi*10^-7;                     %permability of vacum
9   c=3e8;                             %speed of light
10  f=10e9;                             %frequency
11  la=c/f;                            %wavelength
12  w = 2*pi*f;                        %angular fequency
13  T = 0:0.0000001:.01;
14  Zr = sqrt((Ur*U0)/(Er*E0))      %intrinsic impedance
15  Yr = ((j*w)/c)*(sqrt(Er*Ur));   %The propagation constant
16
17  Zin=(Zr*tanh(Yr*T));               %input impedance
18
19
20  %% PLOT
21  figure1 = figure('PaperSize',[20.98 29.68]);
22
23  subplot(2,1,1,'Parent',figure1,...
24      'XTickLabel',{'0␣␣␣␣','1mm','2mm','3mm','4mm','5mm','6mm','7mm','8mm','9mm','10mm'});
25  box('on');
26  grid('on');
27  hold('all');
28  plot (T, real(Zin))
29  xlabel('Thickness␣T')
30  ylabel('Real␣part')
31  subplot(2,1,2,'Parent',figure1,...
32      'XTickLabel',{'0␣␣␣␣','1mm','2mm','3mm','4mm','5mm','6mm','7mm','8mm','9mm','10mm'});
33  box('on');
34  grid('on');
35  hold('all');
36  plot (T, imag(Zin))
37  xlabel('Thickness␣T')
38  ylabel('Imaginary␣part')
```

A.3.2 Combination calculations

```
clear all;
clf
%% Constants
Er = 10.5 - j*0.3;
Ur = 1.2-j*0.5;                 %permability
E0=8.8541878176e-12;              %permittivity of vacum
U0=4*pi*10^-7;                    %permability of vacum
c=3e8;                            %speed of light
f=10e9;                           %frequency
la=c/f;                           %wavelength
w = 2*pi*f;                       %angular fequency
Z_LNG = 292;
Z0 = 377;
Z_par = 251;
T = 0:0.0000001:.01;              %
k = 0:0.00001:1;

Zr = sqrt((Ur*U0)/(Er*E0));       %intrinsic impedance
Yr = ((j*w)/c)*(sqrt(Er*Ur));     %The propagation constant depends on the radar frequency
Z=(Zr*tanh(Yr*T));                %input impedance

%% Combination with given thickness.
t1=2.0/1000;          %imag = 0    re=412.8
t2=4.0/1000;          %imag=0      re=109.3
t3=6.00/1000;         %imag=0      re=174

Z1=(Zr*tanh(Yr*t1));          %input impedance
Z2=(Zr*tanh(Yr*t2));
Z3=(Zr*tanh(Yr*t3));

%% LNG %%
Gamma1=((Z1)-Z_LNG)/((Z1)+Z_LNG);     %Reflection coeff with LNG with given thickness
Gamma3=((Z3)-Z_LNG)/((Z3)+Z_LNG);

Gamma_t1_t3 = k.*Gamma1 + (1-k).*Gamma3;

%% PARAFFIN %%

Gamma1_par=((Z1)-Z_par)/((Z1)+Z_par)
Gamma3_par=((Z3)-Z_par)/((Z3)+Z_par);

Gamma_par = k.*Gamma1_par + (1-k).*Gamma3_par;

%% PLOT %%
figure(1)
    plot(k, real(Gamma_t1_t3))
    title ('Ratio of combination with t=2mm and t=6mm')
    xlabel('Ratio k')
    ylabel('Real part of summarized reflection , real ( \Gamma_\Sigma)')
    axis([0 1 -0.25 0.2])
    grid on

figure(2)
    plot(k, real(Gamma_par))
    title ('Ratio of combination with t=2mm and t=6mm')
    xlabel('Ratio k')
    ylabel('Real part of summarized reflection , real ( \Gamma_\Sigma)')
    axis([0 1 -0.25 0.2])
    grid on

%% Gamma values for given $k_2$

%Gamma12 = 0.7728*Gamma1 + (1-0.7728)*Gamma2
Gamma13 = 0.5949*Gamma1 + (1-0.5949)*Gamma3

%Gamma12_test = 0.6*Gamma1 + (1-0.6)*Gamma2
Gamma_par_test = 0.4*Gamma1_par + (1-0.4)*Gamma3_par
```

A.3.3 Measurements with air

```
clear all
clf
%% DATA IMPORT %%%
s11 = importdata('Type1_luft.d1', ',', 9);
s11Real = s11.data(:,1);
s11Imag = s11.data(:,2);

s11_2 = importdata('Type2_luft.d1', ',', 9);
s11Real_2 = s11_2.data(:,1);
s11Imag_2 = s11_2.data(:,2);

s11_refmet = importdata('refmet.d1', ',', 9);
s11_refmetReal = s11_refmet.data(:,1);
s11_refmetImag = s11_refmet.data(:,2);


%%  BACKSCATTER %%%
refl = (s11Real - j*s11Imag);
refl_2 = (s11Real_2 - j*s11Imag_2);
refl_refmet = (s11_refmetReal - j*s11_refmetImag);


%%  CONSTANTS %%%
N = length(refl);
n = 1:N;

freq = 9+2*1602/1601*(n-1)/N;
c = 300;
k = 2*pi*freq/c;
F = c/sqrt(1)/2/(freq(N)-(2*freq(1)-freq(2)));
bw = freq(N)-(2*freq(1)-freq(2));
%hann = 2*sin(pi*n/N).^2;


%%  ANALYSis / TRANSFORM %%%
han = 2*sin(pi*(n-1/2)/N).^2;
analyse = ifft(refl');
analyse_2 = ifft(refl_2');
analyse_refmet = ifft(refl_refmet');

analysehan_refmet = 2*ifft(han.*refl_refmet');
powhan_refmet = (abs(analysehan_refmet).^2);
[a b] = max(powhan_refmet);
cog_refmet = b-1 + sum((-2:2).*powhan_refmet(b-2:b+2))/sum(powhan_refmet(b-2:b+2))
Pcog = 2/3*sum(powhan_refmet(b-2:b+2))

analysehan = 2*ifft(han.*refl');
powhan = (abs(analysehan).^2);
[a b] = max(powhan(20:30));
b= b+19
cog = b-1 + sum((-2:2).*powhan(b-2:b+2))/sum(powhan(b-2:b+2))

analysehan_2 = 2*ifft(han.*refl_2');
powhan_2 = (abs(analysehan_2).^2);
[a b] = max(powhan_2(20:30));
b= b+19
cog_2 = b-1 + sum((-2:2).*powhan_2(b-2:b+2))/sum(powhan_2(b-2:b+2))


%% FILTER %%%%
analysefilt = analysehan;
analysefilt(1:20)=zeros(size(1:20)); analysefilt(31:1601)=zeros(size(31:1601));

analysefilt_refmet = analysehan_refmet;
analysefilt_refmet(1:20)=zeros(size(1:20)); analysefilt_refmet(31:1601)=zeros(size(31:1601));

analysefilt_2 = analysehan_2;
analysefilt_2(1:20)=zeros(size(1:20)); analysefilt_2(31:1601)=zeros(size(31:1601));

```

```
%% SHIFT %%%%
  reflfilthan = fft(analysefilt);
  reflfilt = reflfilthan.*(1./han);  %fjerner hanning
  reflfiltBand = reflfilt;
  reflfiltBand(1:100)= zeros(size(1:100));
  reflfiltBand((1601-100):1601)=zeros(size((1601-100):1601));
  reflshift = reflfiltBand.*exp(j*2*pi*cog_refmet*n/N);

  reflfilthan_refmet=fft(analysefilt_refmet);
  reflfilt_refmet = reflfilthan_refmet.*(1./han);
  reflfiltBand_refmet = reflfilt_refmet;
  reflfiltBand_refmet(1:100)= zeros(size(1:100));
  reflfiltBand_refmet((1601-100):1601)=zeros(size((1601-100):1601));
  reflshift_refmet = reflfiltBand_refmet.*exp(j*2*pi*cog_refmet*n/N);

  reflfilthan_2=fft(analysefilt_2);
  reflfilt_2 = reflfilthan_2.*(1./han);
  reflfiltBand_2 = reflfilt_2;
  reflfiltBand_2(1:100)= zeros(size(1:100));
  reflfiltBand_2((1601-100):1601)=zeros(size((1601-100):1601));
  reflshift_2 = reflfiltBand_2.*exp(j*2*pi*cog_refmet*n/N);

%% IMPEDANCE CALCULATIONS %%

  reflAbs_korr1 = reflshift./(-reflshift_refmet);
  reflAbs_korr2 = reflshift_2./(-reflshift_refmet);
  Zabs_1 = 377*((1+reflAbs_korr1)./(1-reflAbs_korr1));
  Zabs_2 = 377*((1+reflAbs_korr2)./(1-reflAbs_korr2));

%% VSWR CIRCLE %%

s = 1.2;
center = 250*(s+(1/s))/2
radius = 250*(s-(1/s))/2

G=1000;
angle=0:1/G:2*pi;
x1= center +(radius*cos(angle));
y1=radius*sin(angle);

%% PLOT %%
figure(1)

  subplot(2,1,1)
  plot((n-1)*F, 20*log10(abs(analyse)))
  axis([0 3000 -70 0])
  title ('Backscatter in time domain.')
  xlabel('Distance in mm')
  ylabel('Reflection in dB')
  grid
  subplot(2,1,2)
  plot((n-1)*F, 20*log10(abs(analysehan)))%
  axis([0 3000 -70 0])
  title ('Backscatter in time domain with hanningweighing .')
  xlabel('Distance in mm')
  ylabel('Reflection in dB')
  grid


%figure(2)
% plot(freq, angle(reflfilt))%, n , angle(reflshift_refmet), 'r')
  grid on
  title ('Output.')
  xlabel('Frequency [GHz]')
  ylabel('Amplitude')


figure(3)
  plot(freq, real(Zabs_2), freq, imag(Zabs_2))
  axis([9.2 10.8 -100 300])
  legend('Real part', 'Imaginary part')
```

```
141   title ('Measured impedance of the Bottom Absorber Type2.')
142   xlabel('Frequency (GHz)')
143   ylabel('Impedance (Ohm)')
144   grid on
145
146  figure(4)
147  plot(real(Zabs_1), imag(Zabs_1), real(Zabs_2), imag(Zabs_2), 'r', x1, y1, 'black',...
148       real(Zabs_1(801)), imag(Zabs_1(801)), 'or', real(Zabs_2(801)), imag(Zabs_2(801)), 'or')
149  %axis('equal');
150
151   legend('Type1', 'Type2', 'VSWR = 1.2', 'Value at 10GHz')
152   title ('Input Impedance of bottom absorbers vs VSWR circle.')
153   xlabel('Real part (Ohm)')
154   ylabel('Imaginary part (Ohm)')
155  grid
```

A.3.4 Measurements with paraffin

```
1
2  clear all
3  clf
4
5  %% TAR INN S11 VERDIER FOR ALLE MÅLINGENE %%%
6  l = [ 'refmet.d1'; 'DATA11.d1';'DATA00.d1'; 'DATA01.d1'; 'DATA02.d1'; 'DATA03.d1'; 'DATA04.d1';...
7          'DATA05.d1'; 'DATA06.d1'; 'DATA07.d1'; 'DATA08.d1'; 'DATA09.d1'];
8  celldata = cellstr(l);
9  %filnavn = ['refmet.d1'; 'Type1_luft'; 'Type1_3mm.d1'; 'Type1_10mm.d1'; 'Type1_30mm.d1';'Type1_50mm.d1';...
10 %      'Type1_70mm.d1'; 'Type1_80mm.d1'; 'Type1_90mm.d1'; 'Type1_100mm.d1'; 'Type1_150mm.d1'; 'Type1_200mm.d1' ];
11
12 sattLevel = [0 0 3 10 30 50 70 80 90 100 150 200];
13
14 for p = 1:12
15     v = celldata(p);
16
17     s11 = importdata(char(v) , ',', 9);
18     verdier(p) = s11;
19     s11Real = s11.data(:,1);
20     s11Imag = s11.data(:,2);
21     maaling = (s11Real - j*s11Imag);
22     refl(:,p) = maaling;
23 end
24
25
26 %% KONSTANTER %%%
27 N = length(refl(:,1));
28 n = 1:N;
29
30 freq = 9+2*1602/1601*(n-1)/N;
31 c = 300;
32 k = 2*pi*freq/c;
33 F = c/sqrt(1)/2/(freq(N)-(2*freq(1)-freq(2)));
34 bw = freq(N)-(2*freq(1)-freq(2));
35
36 %% ANALYSE / TRANSFORM %%%
37 han = HANN(N)';
38
39 for r = 1:12
40 analysehan = 2*ifft(han.*refl(:,r)');
41 powhan = (abs(analysehan).^2);
42 [a b] = max(powhan(20:30));
43 b = b+19;
44 b_mat(:,r) = b;
45 cog = b-1 + sum((-2:2).*powhan(b-2:b+2))/sum(powhan(b-2:b+2));
46
47 cog_mat(:,r) = cog;
48 avst_mat(:,r) = cog*F;
49 diff_mat(:,r) = avst_mat(:,1) - avst_mat(:,r);
50 Pcog = (2/3)*sum(powhan(b-2:b+2));
51 Pcog_mat(:,r) = Pcog;
52 PcogdB = 10*log10(Pcog);
53 PcogdB_mat(:,r) = PcogdB;
54
55 navn(:,r) = [celldata(r) PcogdB avst_mat(r)/1000 ]
56 end
57
58 avst_mat(10:12) = avst_mat(9) + (avst_mat(10:12)-avst_mat(9))*0.936;
59 ullage_mat = avst_mat(1)-avst_mat;
60
61 %% Values for pkt 3 and 4 %%
62
63 list_number = 11;
64 ullage = cog_mat(list_number)*F;
65 ext=16;
66 M=N*ext; z=(1:M)/ext;
67
68 %pkt 3
69 integrand3 = han.*refl(:,list_number)'; integrand3(N+1:M)=zeros(size(N+1:M));
```

```
avstand3=2*ext*ifft(integrand3); %for pkt 3
powhan_pkt3 = (abs(analysehan).^2);
[amp3 pos3]=max(powhan_pkt3(8:12));
pos3 = pos3 + 7;
cog_pkt3 = pos3-1 + sum((-2:2).*powhan_pkt3(pos3-2:pos3+2))/sum(powhan_pkt3(pos3-2:pos3+2));
amp3=-10*log10(1/amp3)

%pkt 4
integrand = han.*refl(:,list_number)'; integrand(N+1:M)=zeros(size(N+1:M)); %Padding
avstand4=2*ext*ifft(integrand);
powhan_pkt4 = abs(avstand4(floor(20*ext):floor(ext*30))).^2; %i ekko pkt
[amp4 pos4]=max(powhan_pkt4);
pos4 = pos4 + 19;
cog_pkt4 = pos4-1 + sum((-2:2).*powhan_pkt4(pos4-2:pos4+2))/sum(powhan_pkt4(pos4-2:pos4+2))
amp4=-10*log10(1/amp4)

%pkt 5

integrand5 = han.*refl(:,list_number)'; integrand(N+1:M)=zeros(size(N+1:M)); %Padding
avstand5=2*ext*ifft(integrand5);
powhan_pkt5 = abs(avstand5(floor(25*ext):floor(ext*30))).^2; %i ekko pkt
[amp5 pos5]=max(powhan_pkt5);
pos5 = pos5 + 24;
cog_pkt5 = pos5-1 + sum((-2:2).*powhan_pkt5(pos5-2:pos5+2))/sum(powhan_pkt5(pos5-2:pos5+2))
amp5=-10*log10(1/amp5)

%% PLOT %%
figure(1)
plot( sattLevel, PcogdB_mat, [60 100], [-20 -15], 'r' , [60 250], [-20 -20],'r', [100 250], [-15 -15], 'r' )
axis ([0 200 -25 -10])
grid
xlabel('Measured level, mm')
ylabel('Echo amplitude, dB')
title('Echo signal')
legend ('Echo strength', 'Waveguide')

figure(2)
subplot(2,1,1)
plot( sattLevel, (avst_mat(1)-avst_mat), [85 85], [0 250], 'black', [0 200],[0 200], 'r' )
grid
xlabel('Real level, mm')
ylabel('Ullage, dB')
title('Ullage vs real level')
legend ('Ullage vs real level', 'Half the outlet covered', 'zero difference')
subplot(2,1,2)
plot( sattLevel, (avst_mat(1)-avst_mat)-sattLevel)
grid
xlabel('Real level, mm,')
ylabel('Difference, mm')
title('Difference between ullage and real level')
%legend ('Echo strength', 'Waveguide')

figure(3)
plot((z-z(1))*F ,20*log10(abs(avstand4)),ullage,amp4,'or', cog_pkt5*F, amp5, 'or')
axis([0 3000 -80 0])
grid
xlabel('Distance, mm')
ylabel('Echo amplitude, dB')
title('Echo signal')
legend('Echo signal vs. Measured distance','Maximum for the wanted echo')
%figure(4)
%plot(n, 20*log10((2*ifft(han.*refl(:,2)'))))
```

A.3.5 Validation for testing against air

```
clear all;
clf
%% Constants
Er = 10.5 - j*0.3;
Ur = 1.2-j*0.5;                 %permability
E0=8.8541878176e-12;              %permittivity of vacum
U0=4*pi*10^-7;                    %permability of vacum
c=3e8;                            %speed of light
f=10e9;                           %frequency
la=c/f;                           %wavelength
w = 2*pi*f;                       %angular fequency

Z_lng = 292;
Z_par = 251;
Z0 = 377;

T = 0:0.0000001:.01;              %
k = 0:0.00001:1;

%% IMPEDANCE %%
Zr = sqrt((Ur*U0)/(Er*E0));       %intrinsic impedance
Yr = ((j*w)/c)*(sqrt(Er*Ur));     %The propagation constant depends on the radar frequency
Z=(Zr*tanh(Yr*T));                %input impedance

t1=2.0/1000;          %imag = 0    re=412.8
t2=4.0/1000;          %imag=0      re=109.3
t3=6.00/1000;         %imag=0      re=174

Z1=(Zr*tanh(Yr*t1));        %input impedance
Z2=(Zr*tanh(Yr*t2));
Z3=(Zr*tanh(Yr*t3));


%% AIR %%
Gamma1_air=((Z1)-Z0)/((Z1)+Z0)
Gamma3_air=((Z3)-Z0)/((Z3)+Z0);

Gamma_air = k.*Gamma1_air + (1-k).*Gamma3_air;
Z1_air = Z0.*(1+Gamma_air)./(1-(Gamma_air));

%% Paraffin %%
Gamma1_par=((Z1)-Z_par)/((Z1)+Z_par)
Gamma3_par=((Z3)-Z_par)/((Z3)+Z_par);

Gamma_par = k.*Gamma1_par + (1-k).*Gamma3_par;
Z1_par = Z_par.*(1+Gamma_par)./(1-(Gamma_par));

%% LNG %%
Gamma1_lng=((Z1)-Z_lng)/((Z1)+Z_lng)
Gamma3_lng=((Z3)-Z_lng)/((Z3)+Z_lng);

Gamma_lng = k.*Gamma1_lng + (1-k).*Gamma3_lng;
Z1_lng = Z_lng.*(1+Gamma_lng)./(1-(Gamma_lng));

%% PLOT %%
figure(1)
plot(k, real(Z1_air), k, real(Z1_par), 'r', [0 1], [real(Z3) real(Z1)],...
    'black', [.4 .6] , [251 292], 'black o', [.4268], [251],'black x')
title ('Ratio with respectively air and paraffin as reference')
xlabel('Ratio k')
ylabel('Real part of input impedance')
grid on
legend('Impedance vs ratio with air as reference', 'Impedance vs ratio with paraffin as reference',....
'Linear ratio from 414.9 (t=2mm) to 172.7 (t=6mm)','Ratio obtained with EMDS', 'Calculated ratio for paraffin')
axis ([0 1 150 450])
```

A.4 Data Sheet RAM

EMERSON & CUMING
MICROWAVE PRODUCTS

ENEREPRESENTANT FOR NORGE
ODD TVEDT & CO A/S
Damsgårdsveien 59 - 5058 Bergen
Tlf.: 55 59 98 90 - Fax 55 59 98 99

NUMBER EB-300

TECHNICAL BULLETIN

ECCOSORB* SF and SF-U

THIN, FLEXIBLE, RESONANT ABSORBER

Description

ECCOSORB SF and ECCOSORB SF-U are series of thin, flexible, flat-sheet, resonant absorbers which reflect -20 dB or less of normally incident microwave energy at design frequencies in the range of 1 to 40 GHz.

It concerns magnetically loaded silicone (SF) or polyurethane (SF-U) rubber sheets which are designed to be bonded to flat or curved metallic surfaces to reduce the reflectivity in a narrow band of frequencies.

As a silicone or polyurethane, the material is impervious to water and may be used outdoors. However, in corrosive environments its dielectrically loaded counterparts ECCOSORB DSF and DSF-U (Technical Bulletin EB-080) are recommended.

Availability

ECCOSORB SF and SF-U are available in square sheets of 305 mm x 305 mm (12 in x 12 in) with varying thicknesses according to the desired resonant frequency. Grades are designated by a suffix corresponding to the resonant frequency. For example, ECCOSORB SF-10.0 will be resonant at 10 GHz.
The following standard frequency grades are available : 1.0 - 1.5 - 2.0 - 2.5 - 3.0 - 3.5 - 4.0 - 4.5 - 5.0 - 5.5 - 6.0 - 6.5 - 7.0 - 7.5 - 8.0 - 8.5 - 9.0 - 9.5 - 10.0 - 10.5 - 11.0 - 12.0 - 13.0 - 14.0 - 15.0 - 16.0 - 18.0 - 20.0 - 22.0 - 24.0 - 38.0.

On special order the material can also be supplied in other shapes, sizes or frequencies. ECCOSORB SF-U can also be supplied with a self-adhesive backing.

Applications

Applications include :
- lining radar nacelles, particularly where high power is present
- attaching to masts of ships, walls, etc. to reduce reflections and echoes to nearby antennas

EMERSON & CUMING
Microwave Products N.V.
Nijverheidsstraat 7A
2260 Westerlo
BELGIUM

Tel. : +32 (0) 14 56 25 00
Fax : +32 (0) 14 56 25 01
e-mail : ecmwprod@innet.be

- attaching to vehicles to reduce overall radar signature
- lining magnetron housings to prevent detuning
- lining metallic surfaces to attenuate surface currents
- fabricating into tapered shapes for impedance matching in waveguide or microstrip applications.
- suppressing reflections and surface currents inside microwave units, e.g. power amplifiers of mobile telephones, low noise blocks of satellite receivers etc.
- lining of cavity backed and shrouded telecommunication antennas

Properties

	Typical value	
	SF	**SF-U**
Colour	grey	grey
Dimensions	305 x 305 mm	305 x 305 mm
Maximum thickness	6.3 mm	3.15 mm
Maximum weight	28.7 kg/m²	14.4 kg/m²
Tensile strength	0.96 to 4.6 MPa	3.8 to 5.1 MPa
Elongation	20 to 50 %	15 to 80 %
Tear Strength	1.1 to 2.0 N/mm	3 to 18.2 N/mm
Hardness	73 shore A	73 shore A
Thermal conductivity	0.6 to 1.2 W/m.K	0.5 to 1 W/m.K
Maximum service temperature	165°C	90°C
Power handling capability	0.2 W/cm²	0.1 W/cm²

Reflectivity

ECCOSORB SF and SF-U are designed to have a reflectivity of lower than -20 dB relative to a metal plate. As an example, typical reflectivity curves for ECCOSORB SF-U-3.0, SF-U-10.0 and SF-U-16.0 are shown on the following graph.

SF-U

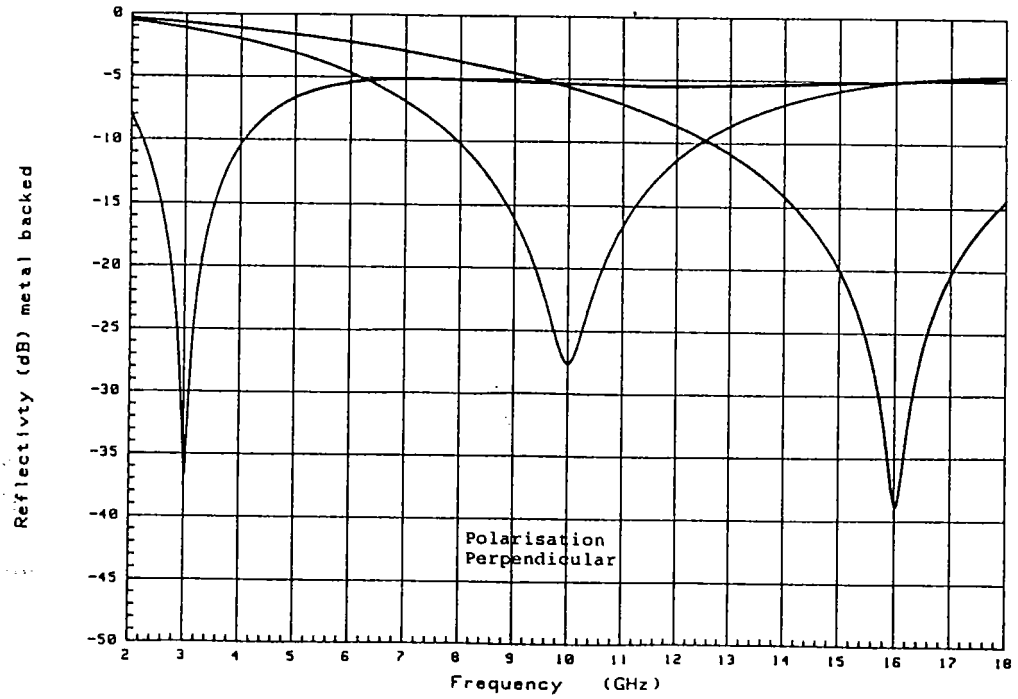

A piece which typically exhibits -25 dB reflectivity at normal incidence will still give -20 dB at an incident angle of 30 degrees, and about -16 dB at 45 degrees. At angles wider than this, performance will degrade at different rates depending upon the polarization, and the resonance frequency will shift slightly higher. This is illustrated by two more plots below showing typical reflectivity curves of ECCOSORB SF-10.0 at various angles of incidence in both perpendicular (TE) and parallel (TM) polarisation.

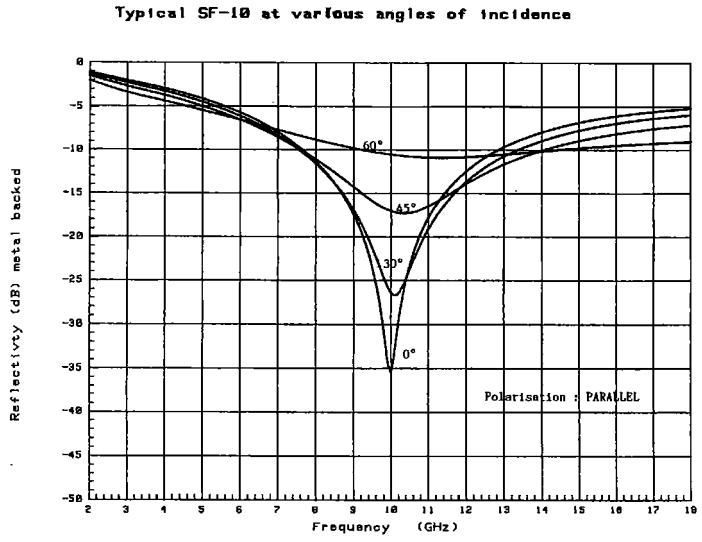

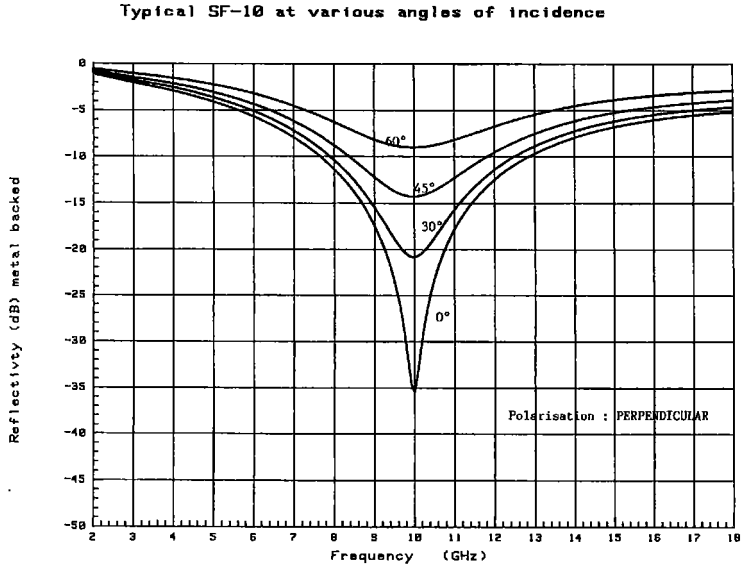

Instructions for use

ECCOSORB SF and SF-U are designed to function directly in front of a metallic surface. If this is not the case, a metallic foil should first be bonded to the object.

To obtain a strong bond of the absorber to the object, the metallic surface should be first thoroughly cleaned with a degreasing solvent. ECCOSORB SF-U can be bonded easily by using ECCOSTOCK* Adhesive 5124 (Technical Bulletin EK-160). The bonding of ECCOSORB SF is more elaborate. After the cleaning and drying of the surface a thin coat of PRIMER* S-11 is applied to the metal and allowed to dry for at least half an hour. Coverage of this primer is about 20 m^2/kg (97 ft^2/lb).

ECCOSIL* 4952 is a two part RTV silicone rubber paste which should be applied in about 90 minutes after being mixed with the catalyst (0,1 - 0,5 %). ECCOSIL 4952 (2 m^2/kg or 9.7 ft^2/lb) is then applied over the primer on the metal surface and onto the back of the ECCOSORB SF sheet which is then pressed into place. The sheet should be held under slight pressure until the cure is complete (usually 18 hours at room temperature). Optimal properties of the bonding rubber will be developed at room temperature after 4 to 6 days.

For more information, see separate technical bulletins for PRIMER S-11 and ECCOSIL 4952 of GRACE N.V.

ECCOSORB SF or SF-U can be readily cut with a sharp knife and template. It is a very flexible material and will conform to mild curvatures. For complex curves, the material may be cut into smaller pieces which are fit into place.

For the reduction of specular reflectivity, performance is highly dependent upon thickness. Therefore the material should not be cut or tapered in any way to change the thickness. However, for the attenuation of surface travelling waves along a metal surface, it may be desirable to machine the leading edge of the absorber in a long gradual taper to improve the impedance match between the uncovered metal and the absorber-covered metal. This will reduce reflected surface waves and scattering at the discontinuity.

Storage Conditions

No special precautions.

Safety Considerations

It is recommended to consult the EMERSON & CUMING MICROWAVE PRODUCTS N.V. product literature, including material safety data sheets, prior to use EMERSON & CUMING MICROWAVE PRODUCTS N.V. products. These may be obtained from your local sales office.

MSWord0197

Warranty

We hope the information given here will be helpful. It is based on data and knowledge considered to be true and accurate and is offered for the user's consideration, investigation and verification; but we do not warrant the results to be obtained. Please read all statements, recommendations or suggestions in conjunction with our conditions of sale **INCLUDING THOSE LIMITING WARRANTIES AND REMEDIES** which apply to all goods supplied by us. We assume no responsibility for the use of these statements, recommendations or suggestions, nor do we intend to use them as a recommendation for any use which would violate statutory obligations or infringe any patent or copyright.